



**ΕΘΝΙΚΟ ΜΕΤΣΟΒΙΟ ΠΟΛΥΤΕΧΝΕΙΟ**  
**ΣΧΟΛΗ ΠΟΛΙΤΙΚΩΝ ΜΗΧΑΝΙΚΩΝ - ΤΟΜΕΑΣ ΓΕΩΤΕΧΝΙΚΗΣ**

Ηρώων Πολυτεχνείου 9, Πολυτεχνειούπολη Ζωγράφου 157 80  
Τηλ: 210 772 3780, Fax: 210 772 3428, e-mail: [gbouck@central.ntua.gr](mailto:gbouck@central.ntua.gr)  
[www.georgebouckovalas.com](http://www.georgebouckovalas.com)

**ΠΡΑΞΗ:**

**«ΘΑΛΗΣ- ΕΜΠ: ΠΡΩΤΟΤΥΠΟΣ ΣΧΕΔΙΑΣΜΟΣ ΒΑΘΡΩΝ  
ΓΕΦΥΡΩΝ ΣΕ ΡΕΥΣΤΟΠΟΙΗΣΙΜΟ ΕΔΑΦΟΣ ΜΕ ΧΡΗΣΗ  
ΦΥΣΙΚΗΣ ΣΕΙΣΜΙΚΗΣ ΜΟΝΩΣΗΣ»**

**MIS 380043**

**Επιστημονικός Υπεύθυνος: Καθ. Γ. ΜΠΟΥΚΟΒΑΛΑΣ**

**ΔΡΑΣΗ 7**

*Εφαρμογή σε Στατικώς Αόριστη Γέφυρα Ο.Σ.*

**ΠΑΡΑΔΟΤΕΑ:**

*Πιλοτικός σχεδιασμός με χρήση «φυσικής» σεισμικής  
μόνωσης (Π7β)*

**Ιούλιος 2015**



**Ευρωπαϊκή Ένωση**  
Ευρωπαϊκό Κοινωνικό Ταμείο



ΕΠΙΧΕΙΡΗΣΙΑΚΟ ΠΡΟΓΡΑΜΜΑ  
ΕΚΠΑΙΔΕΥΣΗ ΚΑΙ ΔΙΑ ΒΙΟΥ ΜΑΘΗΣΗ  
*επένδυση στην κοινωνία της γνώσης*  
ΥΠΟΥΡΓΕΙΟ ΠΑΙΔΕΙΑΣ & ΘΡΗΣΚΕΥΜΑΤΩΝ, ΠΟΛΙΤΙΣΜΟΥ & ΑΘΛΗΤΙΣΜΟΥ  
ΕΙΔΙΚΗ ΥΠΗΡΕΣΙΑ ΔΙΑΧΕΙΡΙΣΗΣ

Με τη συγχρηματοδότηση της Ελλάδας και της Ευρωπαϊκής Ένωσης



**ΕΣΠΑ**  
**2007-2013**  
πρόγραμμα για την ανάπτυξη  
ΕΥΡΩΠΑΪΚΟ ΚΟΙΝΩΝΙΚΟ ΤΑΜΕΙΟ



**NATIONAL TECHNICAL UNIVERSITY OF ATHENS  
SCHOOL OF CIVIL ENGINEERING – GEOTECHNICAL DEPARTMENT**

9 Iroon Polytechniou str., 15780, Zografou Campus, Zografou, Greece  
Tel: +30 210 772 3780, Fax: +30 210 772 3428, e-mail: [gbouck@central.ntua.gr](mailto:gbouck@central.ntua.gr)  
[www.georgebouckovalas.com](http://www.georgebouckovalas.com)

**PROJECT:**

**«*THALIS-NTUA*: INNOVATIVE DESIGN OF BRIDGE PIERS  
ON LIQUEFIABLE SOILS WITH THE USE OF NATURAL  
SEISMIC ISOLATION»**

**MIS: 380043**

**Coordinator: PROF. G. BOUCKOVALAS**

**WORK PACKAGE 7**

*Application to Statically Indeterminate R.C. Bridges*

**DELIVERABLES**

*Pilot Study of a Statically Indeterminate R.C. Bridge pier with  
the new methodology of “natural” seismic isolation (D7b)*

**July 2015**



**European Union**  
European Social Fund



MINISTRY OF EDUCATION & RELIGIOUS AFFAIRS, CULTURE & SPORTS  
MANAGING AUTHORITY

Co-financed by Greece and the European Union



<b>1. Introduction.....</b>	<b>2</b>
<b>2. Brief description of the “natural” seismic isolation methodology.....</b>	<b>4</b>
<b>3. Application to a statically indeterminate RC bridge .....</b>	<b>8</b>
3.1 Conventional bridge design .....	9
3.2 Tolerable settlements and rotations for the statically indeterminate bridge system with shallow foundation .....	10
3.3 Seismic scenarios.....	11
3.4 Design of the shallow foundation .....	13
3.5 Design of the improved “crust”.....	14
3.6 Dynamic impedance functions for footings on liquefiable soil.....	20
3.7 Bridge design.....	26
3.7.1 Operational limit state .....	27
3.7.2 No-Liquefaction case: Seismic scenario B ( $T_{ret}=225y$ ) .....	30
3.7.2.1 Pier reinforcement.....	32
3.7.2.2 Pier confinement.....	32
3.7.2.3 Bearings and Expansion Joints Verification .....	33
3.7.2.3.1 Bearings verification .....	33
3.7.2.3.2 Expansion joints verification .....	36
3.7.3 Liquefaction case: Seismic scenario A ( $T_{ret}=1000y$ ).....	37
3.7.3.1 Horizontal liquefaction-induced differential displacements .....	37
<b>4. Summary and Conclusions.....</b>	<b>48</b>
<b>5. References.....</b>	<b>49</b>

—

# 1. Introduction

---

This Technical Report constitutes **Deliverable #7** of the Research Project titled:

**THALIS-NTUA (MIS 380043)**

**Innovative Design of Bridge Piers on Liquefiable Soils with the use of Natural Seismic Isolation**

carried out under the general coordination of Professor George Bouckovalas, NTUA (Principal Investigator). It presents the work and the corresponding results on tolerable ground deformations carried out for Work Package WP7, titled: “**Application to statically indeterminate RC bridges**”

The Scope of **Work Package WP7**, has been described in the approved Research Proposal as follows:

*“The aim of this WP is to explore the feasibility of the proposed new design methodology, and the resulting advantages over conventional design methods, in the case of a statically indeterminate RC bridge (with continuous box-girder type deck). The main work tasks required to achieve this aim are the following:*

**(a)** *Initially, the allowable foundation movements (settlements and rotations) will have to be established for a statically indeterminate RC bridge system, in terms of the tolerable damage and serviceability level (e.g. driving discomfort, repairable damage, irreparable damage) and the anticipated seismic hazard level (e.g. seismic excitation with 90, 450 or 900 years return period). The allowable foundation movements will result from a joint evaluation of:*

- *an extensive survey of relevant codes and guidelines (e.g. Eurocode 2-Part 2, Eurocode 8-Part 2, Eurocode 7, MCEER & FHWA-chapter 11.4),*
- *examples of actual bridge performance during recent earthquakes, and*
- *parametric (theoretical and/or) experimental studies of various bridge components (e.g. piers, bearings) under static and cyclic-dynamic loading.*

**(b)** *Next, an actual bridge will be selected, with continuous deck system, long spans*

*between piers (in excess of 40m) and extensive liquefiable soil layers underneath one or more of the bridge piers. Note that, following an initial survey, we have already identified a number of such bridges constructed as part of the Egnatia Motorway in Northern Greece, such as the large bridge on Nestos River, with approximately 500m length, and a number of shorter bridges along the motorway connection with the City of Serres. The piers of the selected bridge will be (re-)designed using the conventional foundation approach, i.e. pile groups with ground improvement between and around the piles.*

*(c) Finally, the static and seismic design of this bridge will be repeated with the new methodology of “natural” seismic isolation (i.e. shallow foundation and partial improvement of the top part only of the liquefiable soil), in connection with the allowable foundation movements which were established in work task (a) above. The comparative advantages and limitations of the new design methodology, relative to the conventional one, will be consequently evaluated on the basis of structural performance, as well as cost, criteria.*

The work described herein corresponds to Work task (b) above. It has been carried out by the following members of the **Aristotle University of Thessaloniki (Department of Civil Engineering) Research Team:**

- **Andreas Kappos**, Professor
- **Anastasios Sextos**, Associate Professor

## 2. Brief description of the “natural” seismic isolation methodology

---

Motorway bridge piers are often founded on fluvial and alluvial soil deposits consisting of loose, saturated sands and silty sands as they frequently cross bodies of water such as rivers, streams and lakes. These deposits are generally weak and/or soft enough and conventional design approaches require the construction of deep foundations to avoid excessive settlements or damages due to phenomena such as erosion and scour. Furthermore, in seismically active environments, loose, saturated soil deposits are susceptible to soil liquefaction. In common usage, liquefaction refers to the loss of shear strength in saturated, cohesionless soils due to the build-up of pore water pressures during dynamic loading.

The common practice for designing bridges built on liquefaction-susceptible soils is to construct deep (pile) foundation systems along with extensive improvement of the surrounding soil (**Figure 2.1, left**). Based on the current state of knowledge, deep foundations appear to be the only adequately safe, albeit conservative, solution, resulting to a significant increase in the project cost, compared to cases where shallow foundations could be used [FHWA (1982), FHWA (1987), Sargand and Masada (2006)]. Conventional seismic isolation methods aim to mitigate structural damage by isolating the structure from earthquake ground motions through energy absorption and modification of the structural properties (using for instance, lead rubber, steel neoprene/rubber and fiber-reinforced, elastomeric bearings, combined sliding or elastomeric bearings with fluid dampers, as well as passive and active mass damping systems). The idea proposed herein suggests a fluidizable foundation isolation system intentionally designed to directly reduce the induced seismic ground motions transmitted to the structure (**Figure 2.1, right**). The underlying physical concept is that shear waves can hardly propagate through a fluidized medium; hence, a liquefied soil

layer may act as a seismic isolation barrier to the upward propagating seismic waves. To maintain the bearing capacity of the shallow foundations of the bridge, a non-liquefiable surface “crust” needs also to be assured, in the form either of a non-liquefiable (e.g. clay) layer or an improved ground zone.

Given the particular characteristics of the proposed methodology, it is evident that the current seismic code framework is not adequate for designing bridges with shallow foundations on liquefaction-susceptible soils. Hence, the design process needs to be tailored to the salient features of the novel soil isolation concept, while at the same time complying with the legislative requirements of seismic code provisions. The procedure given in detail in Deliverable 7 [WP07] is applied herein for the case of a statically indeterminate RC bridge. This methodology involves initial design of the superstructure and a shallow foundation according to modern seismic codes (the Eurocodes are used in the present study) with due tailoring to account for the effect of liquefaction on the design seismic loads and displacements.

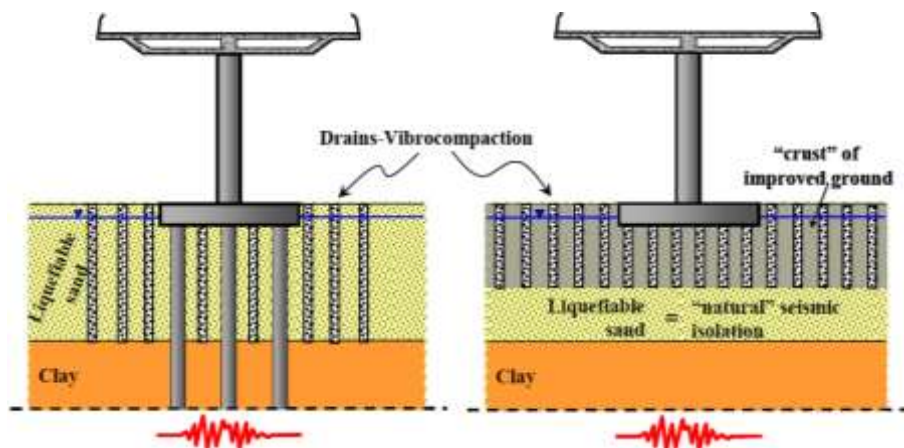


**Figure 2.1.** Bridge design on liquefaction susceptible soils (a) common practice (left) and (b) according to Bouckovalas et al. (2014a) (right).

**Σχήμα 2.1.** Σχεδιασμός γεφυρών σε ρευστοποιήσιμα εδάφη (α) συμβατική προσέγγιση (αριστερά) και (β) σύμφωνα με τη μεθοδολογία των Bouckovalas et al. (2014a) (δεξιά).

Along these lines, the aim of the proposed research is to present a novel methodology for seismic design of low cost bridge foundations on liquefiable soils underlain an intact “crust”. **Figure 2.2** presents a flow chart of the proposed methodology. The key milestones with brief reference to the associated Deliverables and Work Packages of the current project are listed below:

- (a) *Conventional design* of the selected bridge founded on liquefaction-susceptible soil. Based on Eurocode provisions, appropriately designed pile groups are used along with extensive improvement of the surrounding soil [Deliverable 7a, WP07].
- (b) Analytical estimation of the *tolerable settlements and rotations* of the studied bridge. Tolerable settlements and rotations are defined based on performance criteria associated with the acceptable damage level at the bridge [Deliverable 7b, WP07].
- (c) Estimation of the *seismic ground motion* (PGA, PGV and design spectra) considering the non-linear response of the liquefied soil layers [Deliverable 4, WP04].
- (d) *Analytical expressions* for the frequency-dependent parameters of the soil springs and dashpots which will have to be attached at the base of the superstructure in order to simulate the interaction of the foundation with the pre-liquefied and the post-liquefied subsoil [Deliverable 5, WP05].
- (e) *Bridge design* considering static, seismic and liquefaction-induced horizontal differential displacements between the abutments and the adjacent piers [Deliverable 7c (presented herein), WP07].

The application of the novel methodology for the case of a statically indeterminate RC bridge is presented in the following.

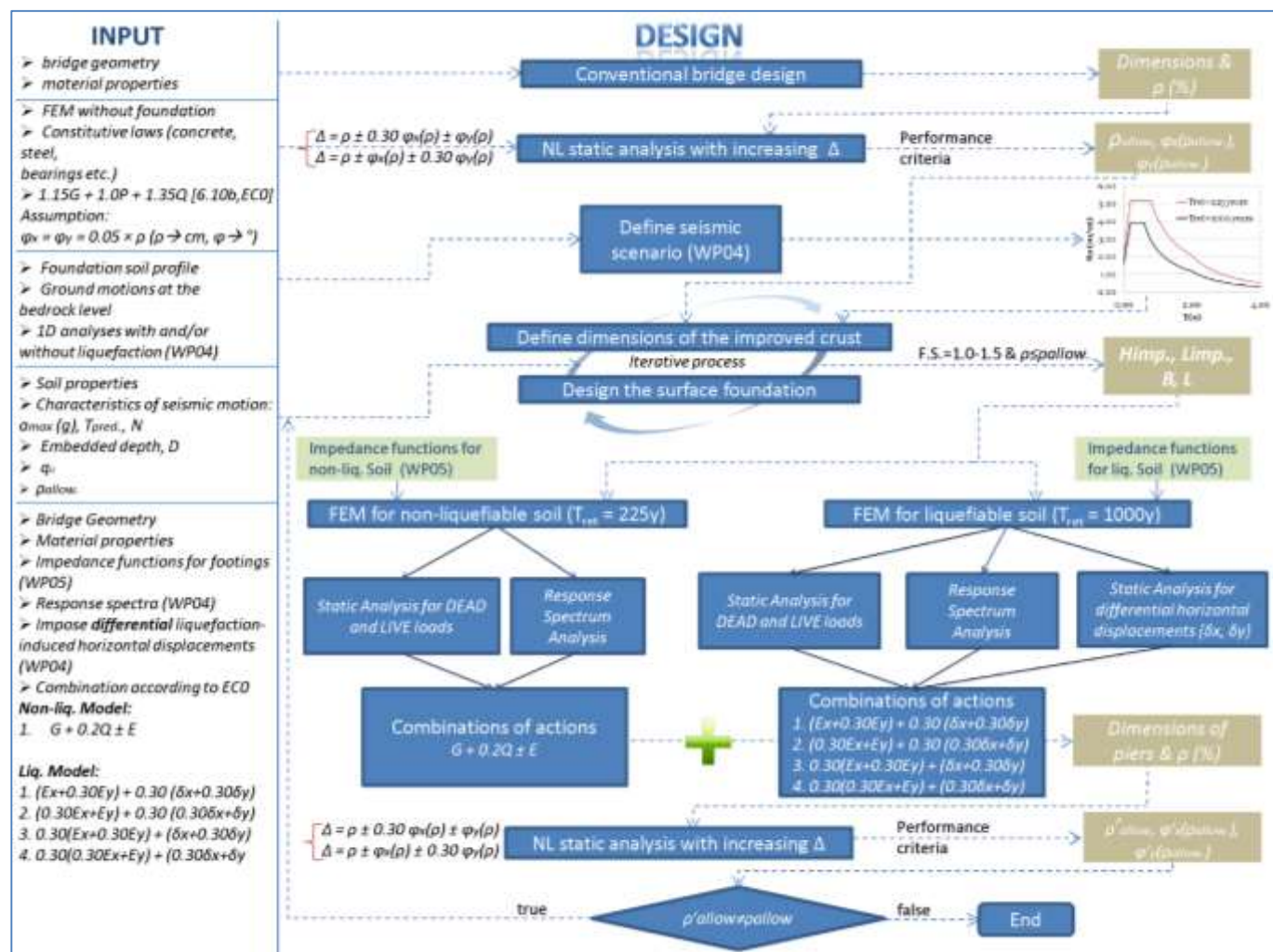


Figure 2.2. Flow chart of the proposed methodology for bridge design on liquefaction-susceptible soils.

Σχήμα 2.2. Διάγραμμα ρής της προτεινόμενης μεθοδολογίας σχεδιασμού γεφυρών σε ρευστοποιήσιμα εδάφη.



### 3.1 Conventional bridge design

Based on the geotechnical study [Deliverable 4, WP04] the soil profile at the site of interest is located within the bed of Strymonas River in Greece and consists mainly of river deposits. More precisely, loose, liquefiable silty sands and soft clays are met while the ground water table is located on the ground surface, a fact that is further enhancing the liquefaction susceptibility.

Due to the high uncertainty associated with the liquefaction phenomenon, verification against liquefaction was performed for two possible seismic scenarios corresponding to a liquefaction case and a 'non-liquefaction' case. Namely:

- *Seismic scenario A (liquefaction case):*  $M_w=7.0$ ,  $PGA_b=0.32g$  ( $T_{ret} = 1000yr$ )
- *Seismic scenario B (non-liquefaction case):*  $M_w=6.7$ ,  $PGA_b=0.22g$  ( $T_{ret} = 225yr$ )

Results from both scenarios indicated high risk of extended liquefaction within a depth of 0.0 to 20.0m. Therefore, the subsoil is improved by installing gravel piles through vibro-replacement. To avoid the liquefaction in the selected geotechnical site, a minimum replacement rate  $\alpha_s=19.6\%$  is needed, corresponding to a quadratic gravel pile grid of diameter  $D=0.80m$  with axial distance  $S=1.60m$  and length  $L=24m$ .

As previously mentioned, the common practice for designing bridges built on liquefaction-susceptible soils is to construct deep (pile) foundation systems. In this case, a 3×3 pile group of 15.0m long piles ( $D=1.0m$ ) was adopted connected with a 7.0×7.0×1.5m pile cap.

Linear elastic static and response spectra analyses were then performed for the static and seismic loads acting on the bridge. A full description of the loads is available in Deliverable 7a [WP07]. The finite element model of the studied bridge is illustrated in **Figure 3.2**. It was found that 176Ø25 and 2Ø16/7.5 are required for the longitudinal and the transverse pier reinforcement, respectively. Finally, two sets of elastomeric bearings with dimensions 500x600mm and thickness of rubber equal to 110mm were used at each deck end and an expansion joint AGFLEXJ 140 ( $\pm 70$ ) or similar was chosen based on displacement calculation or an expansion joint AGFLEXJ 200 ( $\pm 100$ ) based on gap calculation. A full description of the bridge design can be found in Deliverable 7a [WP07].

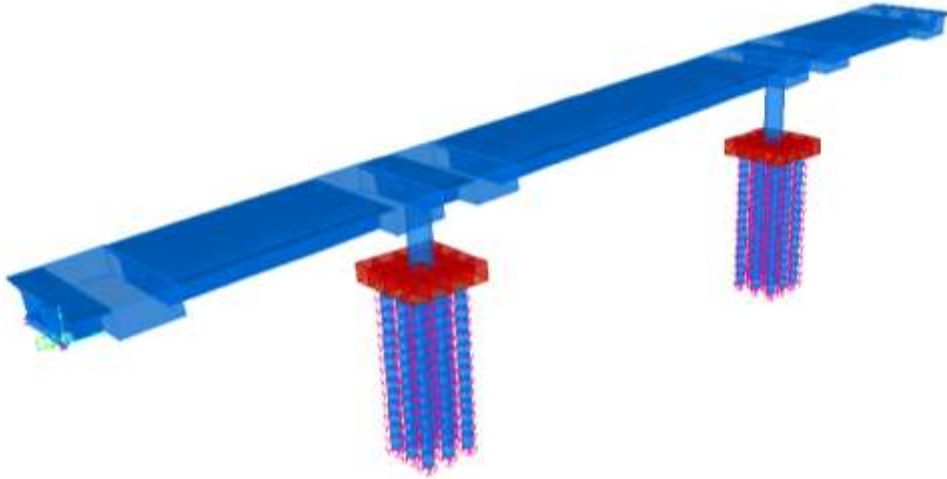


**Figure 3.2:** Finite element model of the bridge.

**Σχήμα 3.2:** Μοντέλο πεπερασμένων στοιχείων της υπό μελέτη γέφυρας.

### 3.2 Tolerable settlements and rotations for the statically indeterminate bridge system with shallow foundation

According to the proposed methodology tolerable settlements and rotations have to be defined for the studied bridge. Tolerable settlements and rotations were derived using nonlinear static analysis. More precisely, a predefined pattern ( $\Delta$ ) of displacements (settlements,  $\rho$ ) and rotations (around the x ( $\vartheta_x$ ) and y ( $\vartheta_y$ ) bridge axes) are applied at the base of the piers until the bridge ‘collapses’. This pattern was defined assuming that settlements and rotations triggered from the liquefaction phenomenon will act as permanent loads in the structure after the earthquake. The following combinations were applied:

$$\Delta = \rho \pm \vartheta_y(\rho) \pm 0.3\vartheta_x(\rho) \quad [3.1]$$

$$\Delta = \rho \pm \vartheta_x(\rho) \pm 0.3\vartheta_y(\rho)$$

Rotations  $\vartheta_y$  and  $\vartheta_x$  were defined as a function of the imposed settlement  $\rho$  according to the empirical equation:

$$\vartheta_x = \vartheta_y = 0.05 \times \rho \quad [3.2]$$

where rotations  $\vartheta_y$  and  $\vartheta_x$  are expressed in [deg] while settlement  $\rho$  is expressed in [cm].

Tolerable settlements were then defined based on performance criteria associated with the acceptable damage level at the bridge. The performance criteria adopted in this case are presented in **Figure 3.3**. Specifically, for settlements ( $\rho$ ) smaller than 0.08m, no damage is expected in the bridge as it responds in the elastic range. For settlements in the range  $0.08 \leq \rho \leq 0.15\text{m}$ , minor damage is expected, while for settlements in the range  $0.15 \leq \rho \leq 0.20\text{m}$ , moderate damage is expected. Finally, the bridge "collapses" for imposed settlements greater than 0.20m. In this case, a value of 0.15m was adopted for the settlements at the base of piers corresponding to minor damage. By further assuming a safety factor of 1.15, the tolerable settlement was set equal to  $0.15/1.15=0.13\text{m}$ . A more detailed description of the adopted procedure is available in Deliverable 7b [WP07].

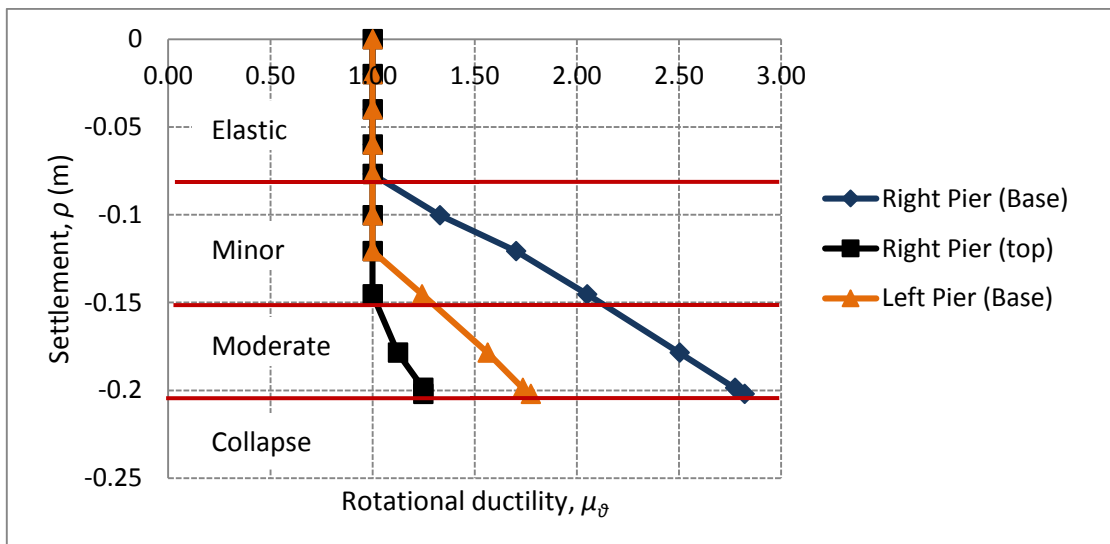


**Figure 3.3.** Applied settlements at the base of piers as a function of rotational ductility.

**Σχήμα 3.3.** Επιβαλλόμενες καθιζήσεις στη βάση των στύλων συναρτήσει της πλαστιμότητας στροφών.

### 3.3 Seismic scenarios

The next step of the proposed methodology requires the generation of design spectra for liquefiable soils for the site of interest. Based on the geotechnical study [Deliverable 4, WP04], response spectra were generated for the two seismic scenarios A (1000yr) and B (225yr). For each scenario, a suite of seven (7) earthquake motions, recorded on bedrock outcrop and having the target magnitude, was selected and properly scaled, for the average response spectrum to match as closely as possible the

design spectra of Eurocode 8 for soil type A, for peak ground acceleration at the bedrock outcrop  $PGA_b = 0.32g$  (Scenario A) and  $PGA_b = 0.22g$  (Scenario B), respectively. Subsequently, one-dimensional, nonlinear site response and liquefaction analyses were performed and the peak intensity measures (PGA, PGV) and the mean 5% damped elastic spectra were derived at the free ground surface. These spectra were then matched with those prescribed in Eurocode 8. The analytical procedure is described in detail in Deliverable 4 [WP04].

**Figure 3.4** presents the elastic response spectra derived for the two examined seismic scenarios for the site of interest. The significant reduction of the ground surface acceleration observed for the liquefaction case ( $T_{ret}=1000y$ ) is attributed to the presence of the liquefiable soil layer. The shear waves can hardly propagate through the fluidized medium, hence, the liquefied soil layer acts as a seismic isolation barrier to the upward propagating seismic waves. Furthermore, the improved crust, located under the footing of the pier, seems to have little impact on the response of the soil surface which is dominated by the liquefiable layer. The resulting response spectra characteristics are then matched to the Eurocode 8 elastic spectra ( $T_{ret}=225y$  with type D and  $T_{ret}=1000y$  with type C). The spectral parameters are summarized in **Table 3.1**. It is further noted that the response spectrum of the vertical component was derived based on Eurocode 8 provisions.

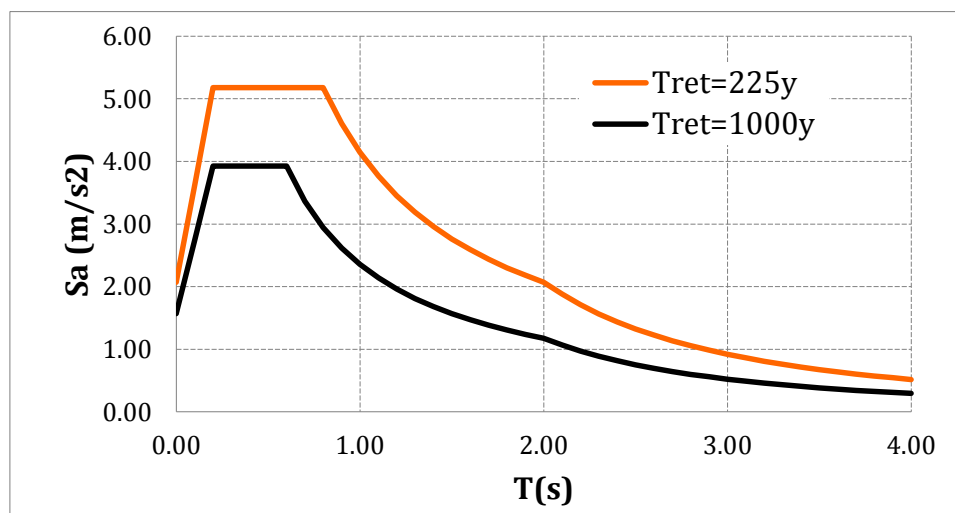


**Figure 3.4.** Elastic response spectra for the two examined seismic scenarios ( $T_{ret}=225y$  and  $T_{ret}=1000y$ ).

**Σχήμα 3.4.** Ελαστικά φάσματα απόκρισης για τα δύο εξεταζόμενα σεισμικά σενάρια ( $T_{ret}=225y$  και  $T_{ret}=1000y$ ).

**Table 3.1.** Elastic spectra characteristics for the two examined seismic scenarios.**Πίνακας 3.1.** Χαρακτηριστικά ελαστικών φασμάτων απόκρισης.

<b>Spectrum characteristics</b>	<b><math>T_{ret}=225</math> years</b>	<b><math>T_{ret}=1000</math> years</b>
<b>EC8 elastic soil</b>	Type D	Type C
<b>Case</b>	No liquefaction	Liquefaction
<b><math>S</math></b>	0.96	0.5
<b><math>T_B(sec)</math></b>	0.2	0.2
<b><math>T_C(sec)</math></b>	0.8	0.6
<b><math>T_D(sec)</math></b>	2	2
<b><math>a_g</math></b>	0.22	0.32
<b><math>A_g</math></b>	2.16	3.14
<b><math>\eta</math></b>	1	1

### 3.4 Design of the shallow foundation

The innovative idea studied herein is that the existence of a surface “crust” of non-liquefiable soil (e.g. clay, dense sand and gravel, or partially saturated-dry soil) with sufficient thickness and shear strength may mitigate the consequences of liquefaction in the subsoil, to such an extent that the use of shallow foundations becomes permissible for bridge structures.

In order to design the improved surface crust and the footing at the bridge piers, the following steps were followed:

- Selection of footing dimensions based on engineering judgement.
- Estimation of the impedance functions at the footing-soil surface according to Mylonakis et al. (2006).
- Response spectrum analysis ( $G+0.2Q\pm E$ ) for the two seismic scenarios described in Section 3.3.
- Check that eccentricity lies within the limits  $L/6 \leq e \leq L/3$ , where  $L$  is the footing length along the examined direction. **According to the geotechnical study, an effort should be made to keep the eccentricity close to  $L/6$ .**
- Improved soil surface zone dimensions are defined considering the dynamic settlements of the soil (Section 3.5) which should not exceed the tolerable settlements derived in Section 3.2.

The above is an iteration process schematically shown in **Figure 3.5** and should be performed along both footing axes until the optimal set of dynamic settlements, improved zone volume and footing dimensions are achieved.

For the case studied, an almost square footing of  $B=9.0\text{m}$  width and  $L=10.5\text{m}$  length corresponding to eccentricities:

- $M_y/N = e_x = B/6.0$
  - $M_x/N = e_y = L/5.80$
- [3.3]

was found to satisfy the predefined eccentricity criteria. Eccentricity check was performed in both directions and both axes were found to be critical due to the sensitivity to torsion of the bridge studied. Thus, an almost square footing is selected to support the structure.

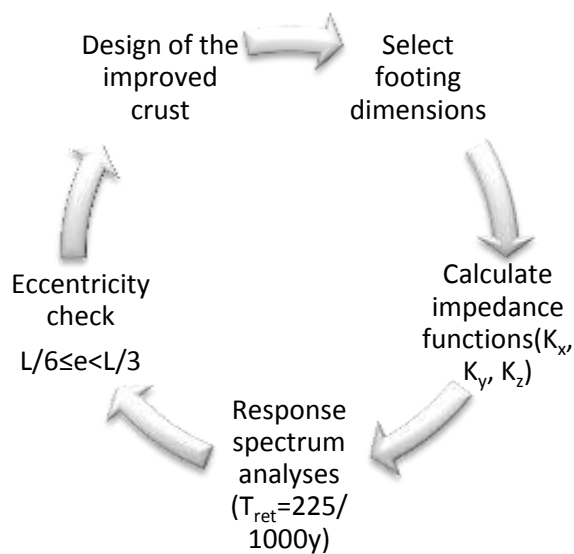


**Figure 3.5.** Iteration process for designing the shallow foundation and the improved soil surface zone.

**Σχήμα 3.5.** Θαμιστική διαδικασία σχεδιασμού της επιφανειακής θεμελίωσης και της επιφανειακής ζώνης βελτίωσης του εδάφους.

### 3.5 Design of the improved “crust”

Focusing on the evaluation of the degraded bearing capacity and the associated seismic settlements of shallow foundations resting on liquefiable soil, an accurate estimation could potentially ensure a viable performance-based design, at least for the case where a sufficiently thick and shear resistant non-liquefiable soil crust exists between the foundation and the liquefiable soil.

The upper part of the surface layer improved using vibro-compaction or vibro-replacement, provides an artificial non-liquefiable crust called the “Equivalent Uniform

Improved Ground” concept (noted hereafter as EUIG), which is widely accepted in practice for the design of geostructures and foundations on weak soil improved with gravel piles. According to EUIG, the improved ground layer is considered uniform with appropriately computed uniform soil parameters, which take into account the properties of the natural ground, the properties of the gravel piles, as well as the extent of ground improvement.

According to Deliverable 3 [WP03] the liquefaction performance of a strip foundation depends on two main factors:

- the seismically induced footing settlements  $\rho_{dyn}$ , and
- the degraded post-shaking bearing capacity of the footing  $q_{ult}$ .

The analytical procedure for the case of a footing resting upon improved soil crust is summarized in the following steps.

Step 1: Determination of the replacement ratio  $\alpha_s$ . The replacement ratio  $\alpha_s$  is estimated considering the initial relative density of the treated soil,  $D_{r,o}$  (%), the thickness of the performed improvement  $H_{imp}$ (m), and the maximum excess pore pressure ratio  $r_{u,max}$  allowed to develop within the improved zone.

Step 2: Determination of the equivalent properties of the improved zone. The permeability,  $k_{eq}$ , and the relative density,  $D_{r,imp}$ , of the improved zone are functions of the replacement ratio  $\alpha_s$  and the initial relative density of the liquefiable sand  $D_{r,o}$  (%).

Step 3: Evaluation of seismic performance of the shallow foundation under conditions of “Infinite” Improvement.

Seismically-induced dynamic settlements  $\rho_{dyn,inf}$ , are evaluated using the Newmark-based relationship:

$$\rho_{dyn}^{inf} = 0.019 \cdot a_{max} (T_{exc} + 0.633 \cdot T_{soil})^2 \cdot (N_0 + 2) \cdot \left( \frac{1}{FS_{deg}^{inf}} \right)^{0.45} \cdot \left[ 1 + 0.25 \cdot \left( \frac{1}{FS_{deg}^{inf}} \right)^{4.5} \right] \quad [3.4]$$

where  $a_{max}$ : peak bedrock acceleration,

$T_{exc}$ : predominant excitation period,

$T_{soil}$ : elastic fundamental period of the soil column,

$N_o$ : number of significant loading cycles,

$FS_{deg,inf}$ : factor of safety, allowing for degradation.

Degraded bearing capacity  $q_{ult,deg,inf}$  is calculated based on the modified analytical relationship initially proposed by Meyerhof & Hanna (1978) as follows:

$$q_{ult,deg}^{inf} = \min \left\{ \begin{array}{l} \frac{1}{2} \cdot \gamma' \cdot B \cdot N_{\gamma 1} \\ \gamma' H_1^2 K_s \frac{\tan \varphi_{1,deg}}{B} + \gamma' [(1 + \alpha^2) - 1] H_1^2 K_s \frac{\tan \varphi_{2,deg}}{B} - \gamma' (1 + \alpha) H_1 + \\ + \frac{1}{2} \gamma' B N_{\gamma 2} + \gamma' (1 + \alpha) H_1 N_{q 2} \end{array} \right\} \quad [3.5]$$

where  $B$  is the footing width,  $H_1$  the thickness of the improved crust and  $\gamma'$  the effective unit weight of the soil, while coefficients  $N_q$  and  $N_\gamma$  are calculated according to Vesic (1973). Between the improved crust and the liquefied sand a transition zone of non-liquefied natural ground (with  $0 < r_u < 1.0$ ) is formed, as a result of the fast dissipation of the earthquake induced excess pore pressures towards the much more permeable improved crust. Coefficients  $\alpha$  and  $K_s$  are associated to the thickness and shear strength mobilized along this transition zone. By reducing the friction angle of the soil, through  $\varphi_{i,deg}$ , the effects of liquefaction and excess pore pressure build-up are considered. The subscript  $i=1$  denotes the friction angle for the improved crust, 2 for the transition zone, and 3 for the liquefied sand.

To further improve the accuracy of the proposed methodology, a correction factor is applied on the initially obtained value.

$$FS_{deg}^{inf} = \frac{FS_{deg}^{inf*}}{0.05 + 0.60(FS_{deg}^{inf*})^{0.85}} > 0.60 FS_{deg}^{inf*} \quad [3.6]$$

where  $FS_{deg}^{inf*}$ : the degraded factor of safety.

**Step 4:** Evaluation of seismic performance of the shallow foundation under conditions of "Finite" Improvement. In real applications, soil improvement is applied over a designated area of limited dimensions. The determination of the particular area should grant the optimum solution between the required performance criteria specified for the shallow foundation and the associated construction costs.

The ratio of  $\rho_{dyn,inf}/\rho_{dyn}$  is analytically evaluated.

$$\frac{\rho_{dyn}^{inf}}{\rho_{dyn}} = 1 - \exp \left[ -1.05 \left( \frac{H_{imp}}{B} \right)^{-1} \left( \frac{L_{imp}}{B} \right)^{0.30} \right] \quad [3.7]$$

where  $H_{imp}$  and  $L_{imp}$  the width and the length of the improvement zone respectively.

The ratio of  $F.S._{deg}/F.S._{deg,inf}$  is computed through the following non-linear equation:

$$\left( \frac{F.S._{deg}}{F.S._{deg}^{inf}} \right)^{-0.45} = \left\{ 1 - \exp \left[ -1.05 \left( \frac{H_{imp}}{B} \right)^{-1} \left( \frac{L_{imp}}{B} \right)^{0.30} \right] \right\} \frac{(F.S._{deg}^{inf})^{4.5} + 0.25 \left( \frac{F.S._{deg}}{F.S._{deg}^{inf}} \right)^{4.5}}{(F.S._{deg}^{inf})^{4.5} + 0.25} \quad [3.8]$$

**Step 5:** Selection of ground improvement dimensions. The ratio of dynamic settlements  $\rho_{dyn}/\rho_{dyn,inf}$  as well as the degradation safety factor,  $F.S._{deg}/F.S._{deg,inf}$  are assessed from design charts [Deliverable 3, WP03] as a function of three different variables,  $L_{imp}/B$ ,  $L_{imp}/H_{imp}$  and  $V_{imp}/B^2$ . **Figure 3.6** illustrates the basic notation for the design of the improved crust.

Based on the recommendations provided in Deliverable 3 [WP03], the improved crust dimensions are defined considering appropriate values for the degradation safety factor  $FS_{deg}$  and the improvement length  $L_{imp}$ . In this study, a value for the safety factor  $FS_{deg}$  greater than 1.10 ( $FS_{deg} \geq 1.10$ ) was deemed acceptable, while an effort was made to minimize the volume of the improved zone  $V_{imp}$  by further keeping the improvement length within (1.4-1.5)  $B$ , where  $B$  is the width of the footing.

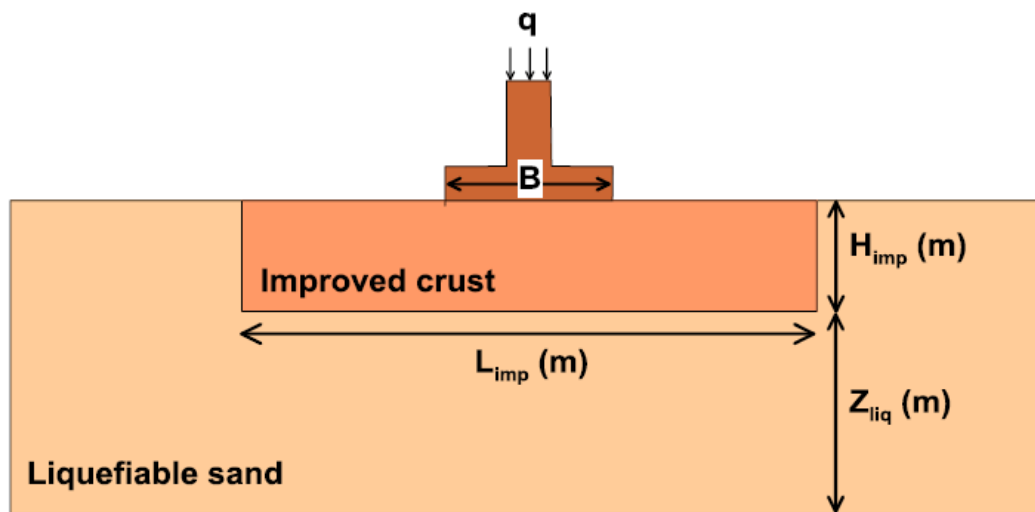


**Figure 3.6.** Notation used for the design of the improved crust.

**Σχήμα 3.6.** Ορισμός βασικών συμβόλων για το σχεδιασμό της βελτιωμένης,

επιφανειακής κρούστας.

The above procedure was then applied for the case of the statically indeterminate bridge considered herein founded on 9.0x10.5m footings. **Table 3.2** summarizes the input data necessary for the design of the improved crust. A trial and error process was performed by gradually modifying the dimensions of the improved zone. Finally, it was found that an improved zone of 14.1m length and 5.5m depth (1.5m embedment depth and 4m improvement) satisfies the predefined criteria ( $FS_{deg}=1.24$ ,  $L_{imp}=1.4B$  and  $V_{imp}=710.64m^3$ ). **Figure 3.7** illustrates the resulting improved zone of 14.1m length and 5.5m depth consisting of a material with relative density 81%, friction angle 40deg and permeability  $1.5 \times 10^{-3}m/s$ . **Table 3.3** summarizes the output of the applied procedure. It is shown that the resulting dynamic settlements are equal to 0.057m, a value that is smaller than the corresponding tolerable dynamic settlement ( $\rho_{dyn}=\rho-\rho_{static}=0.13m-0.02m=0.11m$ ) derived in Section 3.2.

**Table 3.2.** Input data for the design of the improved crust for the case of the statically indeterminate bridge.

**Πίνακας 3.2.** Δεδομένα για το σχεδιασμό της βελτιωμένης επιφανειακής κρούστας για την περίπτωση της στατικώς αόριστης γέφυρας.

Properties		Values
Soil properties	Relative Density of the natural soil, $D_{r,o}$ (%)	60
	Excess Pore Pressure ratio in the improved zone, $r_{u,design}$	0.3
	Buoyant unit weight, $\gamma'$ (kN/m <sup>3</sup> )	9.81
Soil geometry	Total Thickness of the liquefiable layer, $Z_{tot}$ (m)	20
	Thickness of the improved zone, $H_{imp}$ (m)	4
	Thickness of the liquefiable layer, $Z_{liq}$ (m)	14.5
	Width of the improved zone, $L_{imp}$ (m)	12.6
Excitation	Maximum input acceleration, $\alpha_{max}$ (g)	0.17
	Predominant period, $T$ (sec)	0.25
	Number of cycles, $N$	12
Footing properties	Footing width, $B$ (m)	9
	Footing Length, $L$ (m)> $B$ (m) [use 0 for strip footing]	10.5
	Embedment depth, $D$ (m)	1.5
	Total static load from footing, $q_o$ (kPa)	139

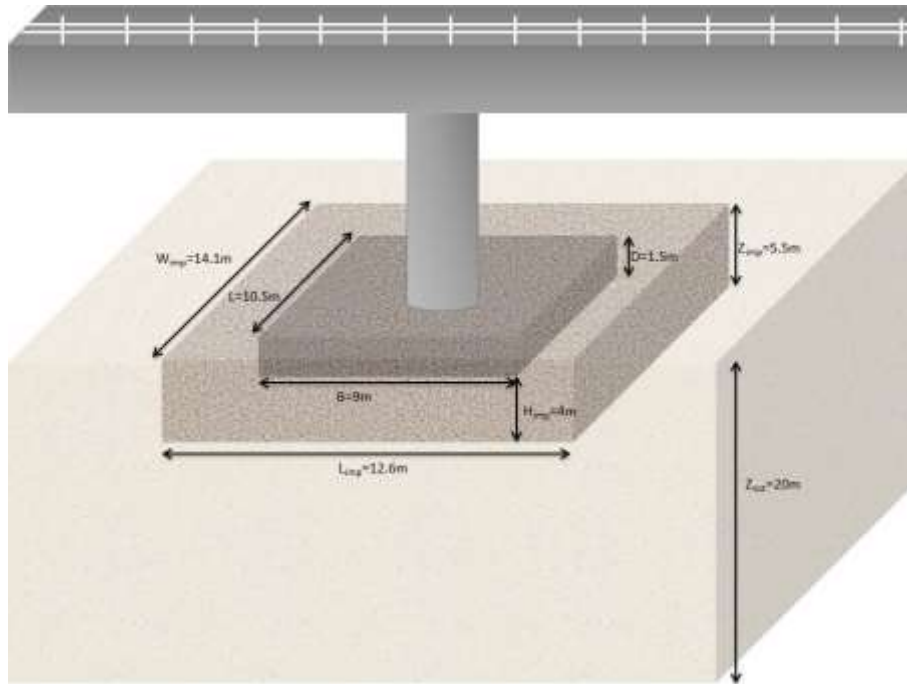


**Figure 3.7.** Layout of the improved zone under the footing of the pier.

**Σχήμα 3.7.** Σχηματοποίηση βελτιωμένης ζώνης κάτω από την επιφανειακή θεμελίωση του μεσοβάθρου.

**Table 3.3.** Soil properties of the improved crust for the case of the statically indeterminate bridge.

**Πίνακας 3.3.** Χαρακτηριστικά της βελτιωμένης επιφανειακής κρούστας για την περίπτωση της στατικής αόριστης γέφυρας.

Properties		Values
Improved soil	Length of the improved zone (m)	14.1
	Volume of the improved zone (m <sup>3</sup> )	710.64
	Replacement ratio, $\alpha_s$	0.132
	Relative Density of the improved zone, $D_{r,imp}$ (%)	81
	Friction Angle of the improved zone, $\varphi_{imp}$ (deg)	40
	Permeability of the improved zone, $k_{eq}$ (m/s)	$1.5 \times 10^{-3}$
	Pore Pressure Ratio below footing, $U3$	0.756
Infinite improvement	Degraded factor of safety, $F.S.^{deg}_{inf}$	1.72
	Seismic settlements, $\rho_{dyn,inf}$ (m)	0.046
	Differential settlements, $\delta$ (m)	0.031
	Rotation, $\vartheta$ (degrees)	0.151
Finite improvement	Degraded factor of safety, $F.S.^{deg}$	1.24
	Seismic settlements, $\rho_{dyn}$ (m)	0.057

	Differential settlements, $\delta$ (m)	0.039
	Rotation, $\vartheta$ (degrees)	0.187

### 3.6 Dynamic impedance functions for footings on liquefiable soil

In order to simulate the foundation-soil interaction analytical expressions are required for the frequency-dependent parameters of the soil springs and dashpots attached to the base of the superstructure. Although this method is well established for non-liquefiable soil profiles, such solutions are not applicable to liquefiable soils due to (a) the existence of multi-layer soil with heavy impedance contrasts between the layers leading to the entrapment of the seismic waves within the liquefied soil layer, and (b) the mostly unknown mechanisms of seismic wave propagation within liquefied soil layers where the effective stresses and the wave propagation velocity may change even within each loading cycle.

Advanced lumped-parameter models, representing the dynamic stiffness of a rigid surface footing resting on liquefiable soil under external harmonic loading, are provided in Deliverable 5 [WP05]. Specifically, a 3-layer soil profile consisting of a surface non-liquefiable crust underlain a loose liquefiable sandy layer resting on a stiff base stratum was considered with sharp impedance contrasts between the layers, leading to strong wave reflections and trapping of energy within the intermediate soft layer (**Figure 3.8**). The dynamic impedance of the footing is expressed by a static component and two dimensionless dynamic modifiers corresponding to a storage stiffness (spring value) and a loss stiffness (damping value). Vertical, horizontal and rocking oscillations are considered leading to three static stiffness components and six dynamic modifiers.

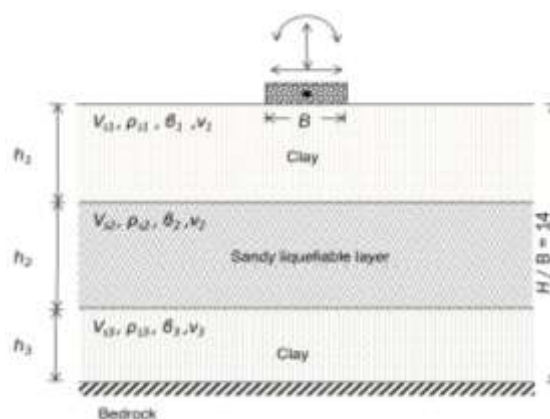


**Figure 3.8.** Layered soil profile consisting of a surface non-liquefiable crust over a loose

liquefiable sandy layer.

**Σχήμα 3.8.** Στρωματοποιημένος εδαφικός σχηματισμός αποτελούμενος από μία επιφανειακή μη ρευστοποιήσιμη κρούστα επί αμμώδους, ρευστοποιήσιμης στρώσης.

Real-time calculations and time domain analysis of non-linear superstructures require lumped-parameter models that represent an unbounded soil domain. The soil-structure interaction of a massless foundation is modelled by assemblies of relatively few springs, dashpots and masses all with real-valued, frequency-independent coefficients. Each degree of freedom at the foundation node of the structural model is coupled to a lumped-parameter model that may consist of additional internal degrees of freedom. The procedure to calculate the springs and dashpots is as follows:

1. Determination of the frequency-dependent impedance or the dynamic stiffness  $S(a_0)$ ,  $a_0$  standing for the familiar dimensionless frequency ( $\omega R/V_S$ ). Note that dynamic stiffness is decomposed into a singular part,  $S_S(a_0)$ , and a regular part,  $S_R(a_0)$ .
2. Approximation of the regular part  $S_R(a_0)$  by the ratio of two polynomials in dimensionless variable ( $i a_0$ ),  $P$  and  $Q$ . The unknown real-valued constant coefficients of the regular part  $S_R(a_0)$  are determined by a curve-fitting technique based on the least-squares method.
3. Establishing the lumped-parameter model from the real coefficients. The lumped-parameter model may contain several zero-order, first-order and second-order discrete element models. The zero-order model contains no internal degrees of freedom (simple springs and dashpots), the first-order model contains one internal degree of freedom (e.g., a spring and a dashpot attached in parallel) and the second-order model contains two internal degrees of freedom (**Figure 3.9**).
4. Finally, the lumped-parameter model is assembled using real-valued springs, dashpots and masses, which can be incorporated directly into dynamic finite element software.

The application of the above procedure to the statically indeterminate RC bridge footings (9.0x10.5m) provides a static component and two dimensionless dynamic

modifiers corresponding to storage (spring) and a loss stiffness (damping) representing the dynamic impedance functions of the footing along the vertical, horizontal and rocking direction.

The analytical expression of the dynamic impedance functions is:

$$K^* = K + i \left( \frac{2\pi}{T} \right) C = k_{static} [k_1(T) + ik_2(T)] \quad [3.9]$$

where  $K = k_{static} \cdot k_1(T)$  denotes the spring coefficient,

$C = k_{static} \cdot k_2(T) \cdot \frac{T}{2\pi}$  is the dashpot coefficient.

Details regarding the static stiffness and the correction factors for cases with and without liquefaction are summarized in **Tables 3.4** and **3.5** respectively.

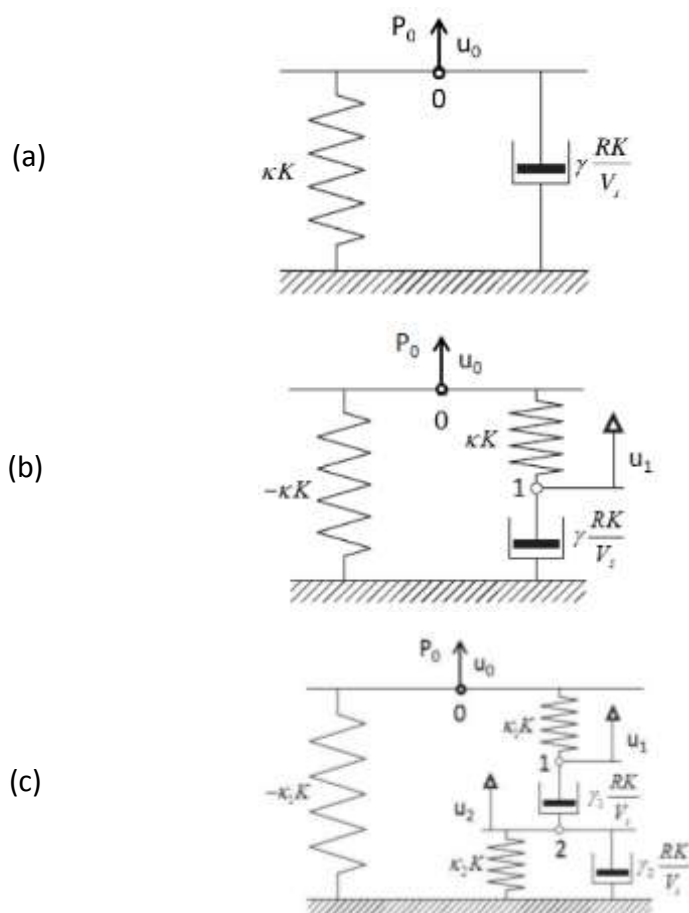


**Figure 3.9.** Discrete element-model for the (a) zero-order, (b) first-order, (c) second-order term.

**Σχήμα 3.9.** Διακριτά προσομοιώματα για όρο (a) μηδενικής, (b) πρώτης, (c) δεύτερης τάξης.

**Table 3.4.** Static component of the spring stiffness for the dynamic impedance.**Πίνακας 3.4.** Τιμή στατικής δυσκαμψίας του δυναμικού συντελεστή εμπέδησης.

Mode	Static Stiffness, $k_{static}$	
	No liquefaction case	Liquefaction case
Vertical, $z$ (kN/m)	2.69E+06	7.21E+05
Horizontal, $y$ (kN/m)	1.93E+06	1.02E+06
Horizontal, $x$ (kN/m)	1.93E+06	1.02E+06
Rocking, $r_x$ (around $x$ axis) (kNm/rad)	4.36E+07	2.67E+07
Rocking, $r_y$ (around $y$ axis) (kNm/rad)	4.36E+07	2.67E+07

**Table 3.5.** Dynamic correction factors for the dynamic impedance. (a) No liquefaction, (b) Liquefaction case.

**Πίνακας 3.5.** Δυναμικοί συντελεστές διόρθωσης του δυναμικού συντελεστή εμπέδησης. (α) Περίπτωση χωρίς ρευστοποίηση, (β) Περίπτωση με ρευστοποίηση.

<b>(a) No liquefaction case</b>														
	<b>k<sub>1</sub>(T)</b>							<b>k<sub>2</sub>(T)</b>						
	<b>T (sec)</b>							<b>T (sec)</b>						
<b>Mode</b>	<b>0.2</b>	<b>0.4</b>	<b>0.6</b>	<b>0.8</b>	<b>1.0</b>	<b>1.25</b>	<b>1.5</b>	<b>0.2</b>	<b>0.4</b>	<b>0.6</b>	<b>0.8</b>	<b>1.0</b>	<b>1.25</b>	<b>1.5</b>
Vertical	0.42	0.68	0.70	0.83	0.87	0.89	0.90	0.88	0.36	0.13	0.06	0.06	0.06	0.06
Horizontal	1.05	0.86	0.87	0.88	0.88	0.92	0.96	0.75	0.55	0.27	0.20	0.14	0.07	0.05
Rocking	0.78	0.92	0.97	0.98	0.99	0.99	1.00	0.27	0.08	0.06	0.06	0.06	0.06	0.06
<b>(b) Liquefaction case</b>														
	<b>k<sub>1</sub>(T)</b>							<b>k<sub>2</sub>(T)</b>						
	<b>T (sec)</b>							<b>T (sec)</b>						
<b>Mode</b>	<b>0.2</b>	<b>0.4</b>	<b>0.6</b>	<b>0.8</b>	<b>1.0</b>	<b>1.25</b>	<b>1.5</b>	<b>0.2</b>	<b>0.4</b>	<b>0.6</b>	<b>0.8</b>	<b>1.0</b>	<b>1.25</b>	<b>1.5</b>
Vertical	0.1	0.64	0.76	0.49	0.52	0.60	0.67	2.50	1.30	1.10	0.80	0.50	0.38	0.28
Horizontal	1.23	1.03	0.97	0.90	0.95	0.91	0.77	1.90	1.10	0.83	0.65	0.56	0.60	0.56
Rocking	0.78	0.88	0.92	0.92	0.93	0.95	0.97	0.54	0.24	0.20	0.14	0.11	0.09	0.07

Note that the above values of damping do not include structural damping under fixed-base conditions.

**Figure 3.10** illustrates the physical interpretation of the dynamic stiffness in the vertical mode of vibration. In this study, the finite element program SAP2000 was used for modelling the bridge. Due to the limited capabilities of the selected software package which does not support frequency-dependent springs and dashpots, the proposed expressions for the dynamic impedance functions cannot be applied directly. Hence, a simplified assumption was made and the impedance function was computed based on the natural frequency of the studied bridge.

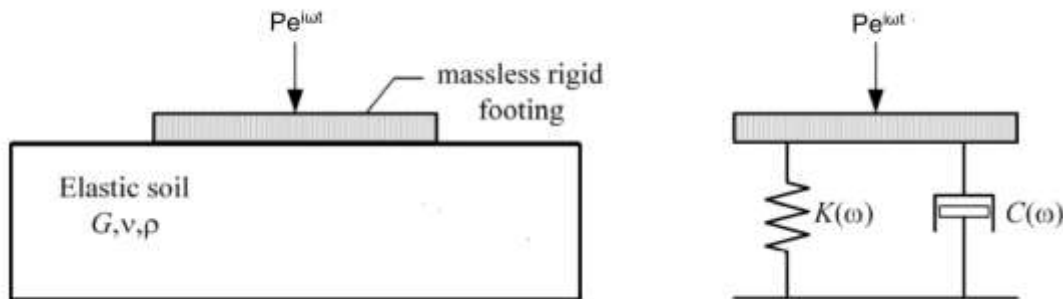
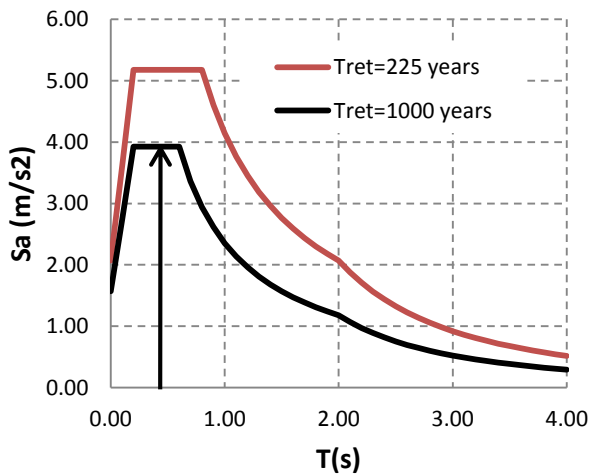


**Figure 3.10.** Vertical oscillation of massless rigid footing on elastic halfspace (left) and physical interpretation of dynamic stiffness in vertical mode of vibration (right).

**Σχήμα 3.10.** Κατακόρυφη διέγερση άκαμπτου, αβαρούς θεμελίου πάνω σε ελαστικό ημίχωρο (αριστερά) και μηχανικό ανάλογο της δυναμικής απόκρισης του εδάφους (δεξιά).



Mode	Period, T (sec)
1 <sup>st</sup>	0.96
2 <sup>nd</sup>	0.79
3 <sup>rd</sup>	0.56

**Figure 3.11.** The translational mode of the structure,  $T_3=0.56$  sec, is located on the plateau of the acceleration spectrum for both scenarios.

**Σχήμα 3.11.** Η μεταφορική ιδιοπερίοδος της κατασκευής,  $T_3=0.56$  sec, αντιστοιχεί στη μέγιστη φασματική επιτάχυνση και για τις δύο περιπτώσεις διέγερσης.

The first three natural frequencies of the bridge are presented in **Figure 3.11**. The first two correspond to a combined translational-torsional mode shape (translation in the transverse direction), while the third one is purely translational along the longitudinal bridge direction. The dynamic impedance functions were computed for the 3<sup>rd</sup> mode shape ( $T_3=0.56$  sec) for the two examined scenarios and are summarized in **Table 3.6**.

**Table 3.6.** Dynamic spring stiffness of the impedance functions for the statically indeterminate bridge considering both load cases, with and without liquefaction.

**Πίνακας 3.6.** Δυναμική δυσκαμψία ελατηρίων των συντελεστών εμπέδησης για τη στατικώς αόριστη γέφυρα και για τις δύο περιπτώσεις φόρτισης, με και χωρίς ρευστοποίηση.

Mode	Stiffness, $K^*$	
	No liquefaction case	Liquefaction case
Vertical, $z$ (kN/m)	1856100	504700
Horizontal, $y$ (kN/m)	1724800	938400
Horizontal, $x$ (kN/m)	1679100	1020000
Rocking, $r_x$ (around $x$ axis) (kNm/rad)	43164000	24030000
Rocking, $r_y$ (around $y$ axis)	41420000	24030000

### 3.7 Bridge design

Having defined (i) the tolerable displacements ( $\rho_{all}$ ) for the specific bridge structure (ii) the response spectra for the particular soil profile for the two examined seismic scenarios (iii) the dimensions ( $B, L$ ) of the footings (iv) the dimensions ( $H_{imp.}, L_{imp.}$ ) of the improved crust and (v) the impedance functions at the pier footing-soil interface, we then proceed to the bridge design.

According to the proposed methodology, due to the high uncertainty level associated with liquefaction, two different finite element models are examined corresponding to the liquefaction ( $T_{ret}=1000y$ ) and non-liquefaction case ( $T_{ret}=225y$ ), respectively. A performance-based design of the bridge is then carried out, explicitly considering two levels of seismic action (two ‘scenarios’) and the corresponding performance objectives. Specifically, for the second seismic scenario ( $T_{ret}=225y$ ) current codes provisions (i.e. Eurocodes) are applied while for the first ( $T_{ret}=1000y$ ), appropriate enhancements are introduced to account for the effect of liquefaction on the design inertial loads and displacements. The application of the performance-based design procedure for the statically indeterminate RC bridge is described in

the following.

### 3.7.1 Operational limit state

First, a refined finite element model is examined considering soil-structure interaction at the base of the piers. The finite element program SAP2000 was used for the analysis of the bridge. Elastic beam elements were used for modelling the deck, piers and piles. The bearings were incorporated in the model with the use of equivalent elastic springs. For elastomeric bearings, the horizontal effective stiffness is determined by the shear modulus of the elastomer ( $G$ ), the full cross-sectional area ( $A$ ) and the total thickness of the rubber layers ( $t_r$ ), i.e.  $K_{eff}=GA/t_r$ . The vertical stiffness ( $K_v$ ) is computed considering the compression modulus  $E_c$  of the elastomer ( $K_v=E_cA/t_r$ ) while the flexural stiffness of the pad is calculated as  $K_b=0.329E_cI/t_r$ , where  $I$  is the moment of inertia of the bearing section [Naeim and Kelly, 1999]. According to EN 1337-1 at a nominal temperature of  $23\text{ }^\circ\text{C} \pm 2\text{ }^\circ\text{C}$  the value  $0.90\text{MPa}$  can be used for the conventional shear modulus of the bearings. The stiffness values derived are summarized in **Table 3.7**.

According to EC8-2 §7.2.4(5), different stiffness values have to be used for the static and the seismic combinations. Thus, for the horizontal springs the stiffness of the bearings is:

#### Static Load Combinations:

$$K_{b,st,H} = \frac{G \cdot A}{t_r} = \frac{0.9 \cdot 10^3 \cdot 0.50 \cdot 0.60}{0.110} = 2455 \text{ kN/m}$$

$$K_{b,st,V} = \frac{E_c \cdot A}{t_r} = 2538621 \text{ kN/m}$$

#### For displacements under seismic load combinations:

$$K_{b,dis,H} = 1.25 \cdot 2455 = 3069 \text{ kN/m}$$

$$K_{b,dis,V} = 1.25 \cdot 2538621 = 3173276 \text{ kN/m}$$

#### For inertial forces under seismic load combinations:

$$K_{b,for,H} = 1.20 \cdot 1.25 \cdot 2455 = 3683 \text{ kN/m}$$

$$K_{b,for,V} = 1.20 \cdot 1.25 \cdot 2538621 = 3807932 \text{ kN/m}$$

**Table 3.7:** Bearing properties

**Πίνακας 3.7:** Ιδιότητες εφεδράνων

$b_x(m)=$	0.50	Characteristics of the bearing
$b_y(m)=$	0.60	
$G(MPa)=$	0.90	
$K(MPa)=$	2000	
$t(m)=$	0.011	
$n(layers)=$	10	
$S=$	12.40	$b_x \times b_y / [2(b_x + b_y)t_r]$
$E_c(MPa)=$	930.83	$6.73 \times G \times S^2$
$E_{c,red}(MPa)=$	635.20	$E_c \times K / (E_c + K)$
$K_v(kN/m)=$	<b>2538621</b>	$E_c \times A / t_r$
$K_h(kN/m)=$	<b>2455</b>	$G \times A / t_r$
$K_{bx}(kNm/rad)=$	<b>17098</b>	$0.329 \times E_c \times I_x / t_r$
$K_{by}(kNm/rad)=$	<b>11874</b>	$0.329 \times E_c \times I_y / t_r$

Soil-structure interaction effects were considered at the base of piers. The static stiffness for the 9.0x10.50m footing was derived according to Poulos and Davis (1974).

$$K_z = \frac{4 \bar{G} R}{1 - \nu} = \frac{4 \times 8.9 \times 10^3 \times 5.50}{1 - 0.3} = 2.8 \times 10^5 \text{ kN/m}$$

$$K_h = \frac{32 (1 - \nu) \bar{G} R}{7 - 8\nu} = \frac{32 \times (1 - 0.30) \times 10.5 \times 10^3 \times 5.50}{7 - 8 \times 0.3} = 2.81 \times 10^5 \text{ kN/m}$$

$$K_r = \frac{8 \bar{G} R^3}{3 (1 - \nu)} = \frac{8 \times 10.5 \times 10^3 \times 5.50}{3 \times (1 - 0.3)} = 6.66 \times 10^6 \text{ kNm/rad}$$

Next, **linear elastic** analysis is performed for the **static** loads acting on the bridge. A full description of the bridge static loads was given in Deliverable 7a [WP07]. Load combinations at the operability limit state (OLS) were then examined [Deliverable 7a, WP07]. **Figure 3.12** illustrates the bending moments and the corresponding axial forces at the ultimate limit state (Combination *OLS1: 1.35G+1.50Q*). The maximum bending moments for this combination at the left and right piers are  $M=7085\text{kNm}$  and  $M=8055\text{kNm}$ , respectively, while the maximum axial forces at the base of the two piers are  $N=-16,638\text{kN}$  and  $N=-16,609\text{kN}$ , respectively.

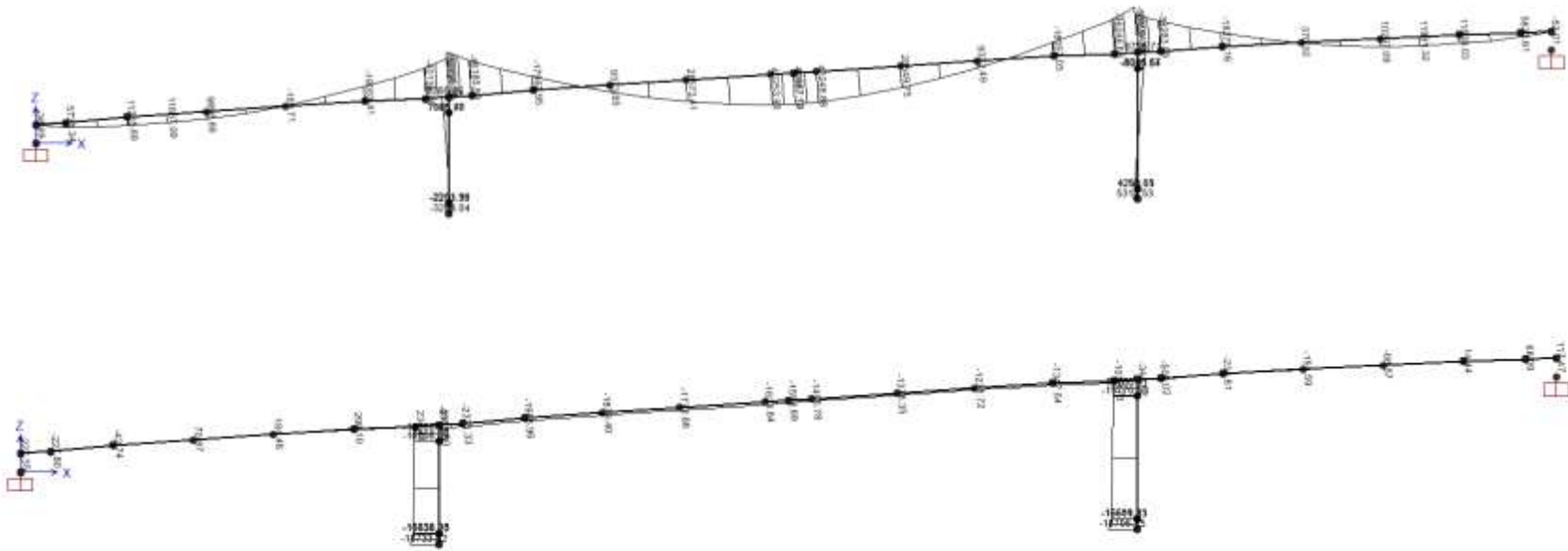


**Figure 3.12.** Bending moments (top) and corresponding axial forces (bottom) acting on the bridge at the ultimate limit state [Combination  $OLS1$ :  $1.35G+1.50Q$  (units:  $kNm$ ,  $N$ )].

**Σχήμα 3.12.** Διάγραμμα ροπών (πάνω) και αντίστοιχων αξονικών δυνάμεων (κάτω) που αναπτύσσονται στη γέφυρα στην οριακή κατάσταση αστοχίας [Συνδυασμός  $OLS1$ :  $1.35G+1.50Q$  (μονάδες:  $kNm$ ,  $N$ )].

### 3.7.2 No-Liquefaction case: Seismic scenario B ( $T_{ret}=225y$ )

In this case a refined finite element model is also examined considering soil-structure interaction at the base of the piers. The finite element model of the bridge was described in Section 3.7.1. The only modification made is with regard to the dynamic impedance functions. The dynamic impedance functions at the footing-soil interface adopted for the no liquefaction case were computed in Section 3.6. The refined finite element model of the studied bridge is illustrated in **Figure 3.13**.

**Response spectrum** analysis was then performed for the earthquake loads defined in Section 3.3. Seismic loads combinations presented in Deliverable 7a [WP07] were then examined. **Figure 3.14** shows the bending moments and the corresponding axial forces for the seismic combination  $G+0.2Q+Ex+0.30Ey+0.30Ez$ . The maximum bending moments for this combination at the left and right piers are  $M=19,178kNm$  and  $M=15,176kNm$ , respectively, while the maximum axial forces at the base of the two piers are  $N=-11,467$  and  $N=-11,803kN$ , respectively.

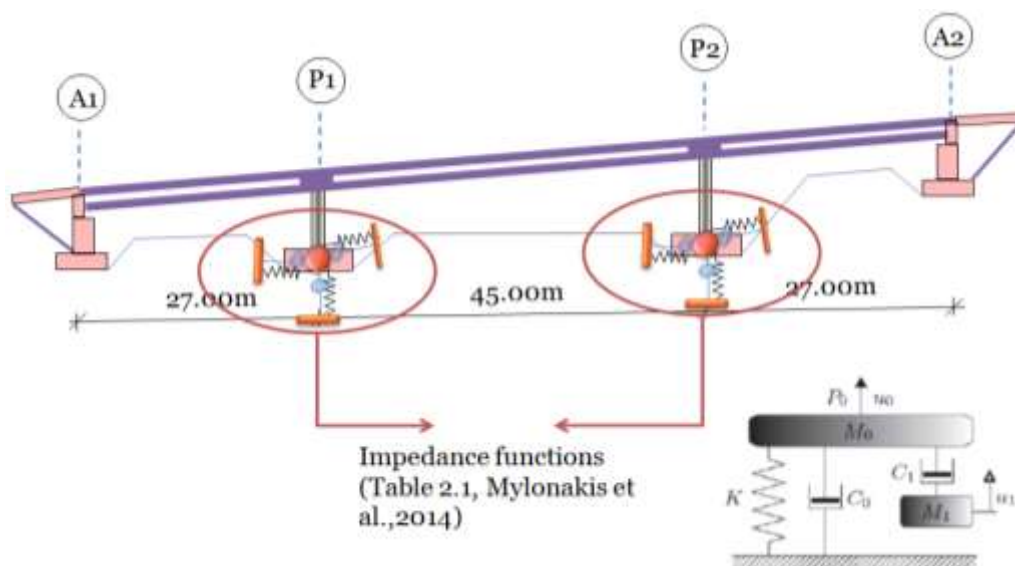


**Figure 3.13.** Refined finite element model for the statically indeterminate bridge.

**Σχήμα 3.13.** Λεπτομερές προσομοίωμα πεπερασμένων στοιχείων της υπερστατικής γέφυρας.

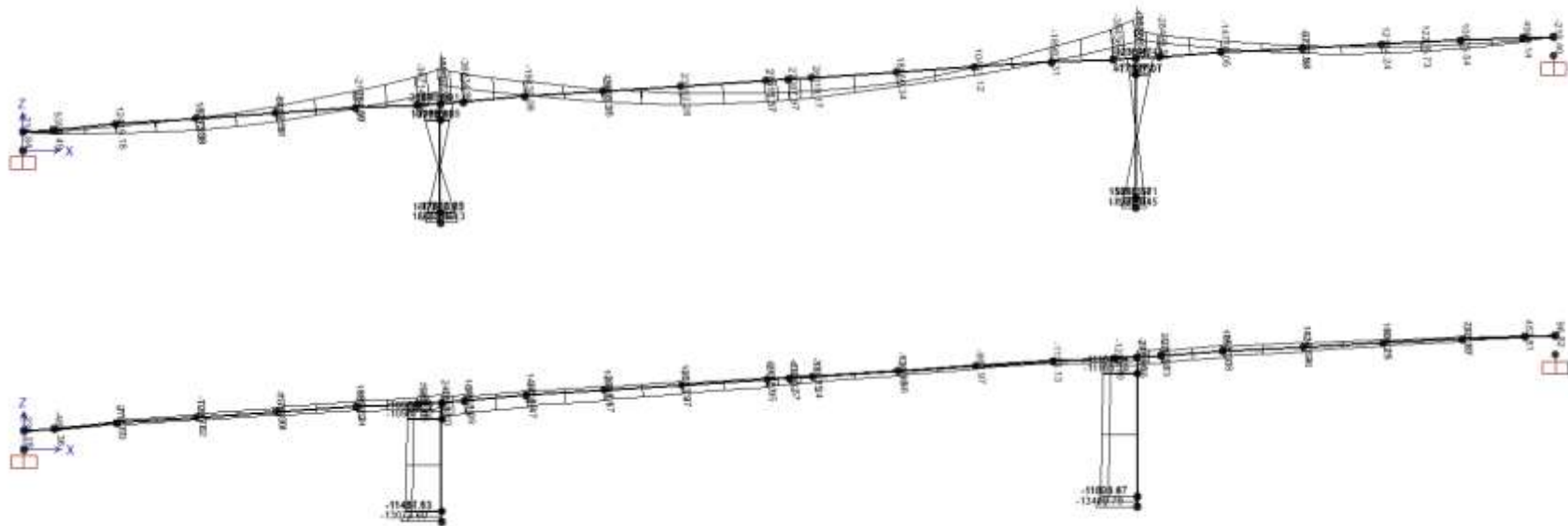


**Figure 3.14.** Bending moments (top) and corresponding axial forces (bottom) acting on the bridge for the seismic combination  $G+0.2Q+Ex+0.30Ey+0.30Ez$  (units:  $kNm$ ,  $N$ ).

**Σχήμα 3.14.** Διάγραμμα ροπών (πάνω) και αντίστοιχων αξονικών δυνάμεων (κάτω) που αναπτύσσονται στη γέφυρα για το σεισμικό συνδυασμό  $G+0.2Q+Ex+0.30Ey+0.30Ez$  (μονάδες:  $kNm$ ,  $N$ ).

### 3.7.2.1 Pier reinforcement

The required reinforcement of the pier is equal to  $907\text{cm}^2$ . The minimum percentage of reinforcement (1%) corresponds to  $314\text{cm}^2$ . Finally,  $146\Phi 25$  ( $717\text{cm}^2$ ) are used for the pier (2.28%).

### 3.7.2.2 Pier confinement

The maximum compressive load of the piers is equal to  $N_c = -16638\text{kN}$ .

Since the normalized axial force  $n_k$  exceeds the limit of 0.08, as:

$$n_k = \frac{N_c}{f_{ck} A_c} = 16638 / (40400 \times 3.14 \times 2.00^2/4) = 0.13 > 0.08$$

confinement should be provided. The minimum amount of confining reinforcement for a spiral is:

$$\omega_{min} = 1.40 \cdot \frac{A_c}{A_{cc}} \cdot \lambda \cdot n_k \geq 0.180 \quad \omega_{min} = 1.40 \cdot \frac{2.0^2}{1.84^2} \cdot 0.37 \cdot 0.13 = 0.08 < 0.18 \rightarrow \omega_{min} = 0.18$$

The required confining reinforcement is defined by the mechanical reinforcement ratio which is:

$$\min \rho_w = \omega_{min} \cdot \frac{f_{cd}}{f_{yd}} = 0.18 \cdot \frac{30000/1.5}{500000/1.15} \Rightarrow \min \rho_w = 0.0083$$

Spirals  $2\Phi 16/10$  are used with a volumetric ratio:

$$\rho_w = \frac{4A_{sp}}{D_{sp} \cdot s_L} = \frac{4 \cdot 2 \cdot 2.0\text{cm}^2}{184\text{cm} \cdot 10.0\text{cm}} \Rightarrow \rho_w = 0.0087 \cong \min \rho_w$$

The spacing of the spiral should satisfy the limits:

$$s_L = 10.0\text{cm} < 6d_{bL} = 6 \cdot 2.5\text{cm} = 15\text{cm} \text{ (where } d_{bL} \text{ is the longitudinal bar diameter) and}$$

$$s_L = 10.0\text{cm} < D_{cc}/5 = 184/5 = 36.8\text{cm} \text{ (where } D_{cc} \text{ is the diameter of the confined concrete core).}$$

### 3.7.2.3 Bearings and Expansion Joints Verification

#### 3.7.2.3.1 Bearings verification

##### Geometrical characteristics

Width	b = 500mm
Length	l = 600mm
Thickness of rubber layers	11mm
No of rubber layers	10
Effective rubber thickness	110mm
Shape coefficient	12.40
Shear modulus G	1.125 MPa
Horizontal stiffness of bearing	$K_h = 3068 \text{ kN/m}$
Vertical stiffness of bearing	$K_v = 1560601 \text{ kN/m}$
Rotational stiffness of bearing	$K_{bx} = 19801 \text{ kNm/rad}$
Rotational stiffness of bearing	$K_{by} = 13751 \text{ kNm/rad}$

##### Loads – displacements – rotations

##### *Vertical loads (compression positive)*

Dead loads	954.9 kN
Super dead loads	250.6 kN
Uniform road traffic loads	82.4 kN
Longitudinal earthquake	238.5 kN
Lateral earthquake	1947.8 kN
Vertical earthquake	347.3 kN

##### Displacement x-x

Displacement due to dead load	1.534 mm
Displacement due to uniform road traffic loads	0.307 mm
Displacement due to temperature	37.34 mm

##### Displacement y-y

Displacement due to dead load	0.00 mm
Displacement due to uniform road traffic loads	0.00 mm
Displacement due to temperature	0.00 mm

##### Rotations

##### **Rotations $\alpha_x$**

Rotation due to dead load	0.00 rad
Rotation due to uniform road traffic loads	0.00 rad
Rotation due to temperature	0.00 rad

**Rotations  $\alpha_y$**

Rotation due to dead load	8.54 × 10 <sup>-4</sup> rad
Rotation due to uniform road traffic loads	0.00 × 10 <sup>-4</sup> rad
Rotation due to temperature	2.53 × 10 <sup>-4</sup> rad

**COMBINATION: G "+" P "+" (Ex+0.30×Ey+0.30×Ez) "+" 0.5×T:**

**Max displacements and rotations of bearing:**

From dynamic analysis	d <sub>Sdx</sub> = 54.54 mm
	d <sub>Sdy</sub> = 57.81 mm
Design displacement x-x	d <sub>Edx</sub> = 74.74 mm
Design displacement y-y	d <sub>Edy</sub> = 57.81 mm
	d <sub>Ed</sub> = 94.49 mm
From dynamic analysis	a <sub>Sx</sub> = 0.00 × 10 <sup>-4</sup> rad
	a <sub>Sy</sub> = 6.00 × 10 <sup>-4</sup> rad
Design rotation x-x	a <sub>Edx</sub> = 0.00 × 10 <sup>-4</sup> rad
Design rotation y-y	a <sub>Edy</sub> = 1.58 × 10 <sup>-3</sup> rad

**Design shear strain**

Check  $\epsilon_d = d_{Ed} / \Sigma t_r < 2.0$  ε<sub>q,d</sub> = 0.86 < 2.0 (ok)

**Design shear strain due to compressive load**

Seismic design displacement	d <sub>Ed</sub> = 94.49 mm
Effective area of bearing in x-x	A <sub>r</sub> = (500-74.74) × (600-57.81)
	= 230572 mm <sup>2</sup>
Max compressive load for design earthquake	N <sub>sd</sub> = 2132.5 kN
Max effective normal stress	σ <sub>ε</sub> = 9249 kN/m <sup>2</sup>
Shear modulus	G = 1.125 MPa
Deformation due to vertical loads	ε <sub>0,d</sub> = 1.5 σ <sub>ε</sub> / (SG) = 0.99

**Design shear strain due to angular distortion**

$\epsilon_{\alpha,d} = (l^2 a_x + b^2 a_y) / (2t_i \cdot \Sigma t_i)$  ε<sub>α,d</sub> = 0.235 rad  
 Check max design strain: ε<sub>q,d</sub> + ε<sub>0,d</sub> + ε<sub>a,d</sub> < ε<sub>u,d</sub> 2.09 < 7.0 (ok)

**COMBINATION: G "+" P "+" (0.30×Ex+Ey+0.30×Ez)+0.5×T**

**Max displacements and rotations of bearing:**

From dynamic analysis	d <sub>Sdx</sub> = 16.36 mm
	d <sub>Sdy</sub> = 192.71 mm
Design displacement x-x	d <sub>Edx</sub> = 36.56 mm
Design displacement y-y	d <sub>Edy</sub> = 192.71 mm
	d <sub>Ed</sub> = 196.15 mm

From dynamic analysis	$a_{Sx} = 3.29 \times 10^{-4}$ rad
	$a_{Sy} = 1.37 \times 10^{-4}$ rad
Design rotation x-x	$a_{Edx} = 3.29 \times 10^{-4}$ rad
Design rotation y-y	$a_{Edy} = 1.37 \times 10^{-3}$ rad

**Design shear strain**

Check  $\epsilon_d = d_{Ed} / \Sigma t_r < 2.0$   $\epsilon_{q,d} = 1.78 < 2.0$  (ok)

**Design shear strain due to compressive load**

Seismic design displacement	$d_{Ed} = 196.15$ mm
Effective area of bearing in x-x	$A_r = (500 - 36.56) \times (600 - 192.71)$ $= 188754 \text{ mm}^2$
Max compressive load for design earthquake	$N_{sd} = 3329.0$ kN
Max effective normal stress	$\sigma_e = 17637$ kN/m <sup>2</sup>
Shear modulus	$G = 1.125$ MPa
Deformation due to vertical loads	$\epsilon_{0,d} = 1.5 \sigma_e / (SG) = 1.26$

**Design shear strain due to angular distortion**

$\epsilon_{\alpha,d} = (l^2 a_x + b^2 a_y) / (2t_i \cdot \Sigma t_i)$   $\epsilon_{\alpha,d} = 0.238$  rad  
 Check max design strain:  $\epsilon_{q,d} + \epsilon_{0,d} + \epsilon_{\alpha,d} < \epsilon_{u,d}$   $3.28 < 7.0$  (ok)

**Check of stability**

$b_{min} = 500 > 4 \cdot 110 = 440$  mm (ok)  
 $\sigma_e = 17.64 \leq \frac{2 \cdot 400}{3 \cdot 110} \cdot 1.125 \cdot 12.40 = 33.81$  MPa (ok)

**Check of anchorage**

$\frac{V_{Ed}}{N_{Ed}} \leq \alpha + \frac{\beta}{\sigma_e}$  and  $\sigma_e \geq 3.0$  N/mm<sup>2</sup>

$V_{Ed} = 436.9$  KN

$\frac{436.9}{3329.0} = 0.13 < 0.5 + \frac{0.6}{12.40} = 0.55$  (ok)

No need for anchorage.

**CHECK FOR STATIC COMBINATIONS (ACCORDING TO DIN4141)**

Total displacement	37.53 mm
Shear strain	$\gamma_d = 0.35 < \gamma_{al} = 0.69$ (ok)
Max normal stress of bearing	$\sigma_{max} = 6.54$ MPa < 15.00 MPa
Min normal stress of bearing	$\sigma_{min} = 5.86$ MPa > 5.00 MPa

**3.7.2.3.2 Expansion joints verification**

**Displacements:**

Braking load	1.59 mm
Uniform difference of temperature $\Delta T = -37^\circ\text{C}$	31.44 mm
Uniform difference of temperature $\Delta T = 57^\circ\text{C}$	37.34 mm
Earthquake x-x	94.49 mm
Earthquake y-y	196.15 mm

For **static** conditions, the design displacement for the loading direction i-i is:

$$d_{Edi} = d_G \pm 1.5 \cdot 0.6 d_T \pm 1.5 d_{BR}$$

where

- $d_G$  : displacement due to permanent or quasi-permanent actions
- $d_T$  : displacement due to temperature actions
- $d_{BR}$  : displacement due to braking

For **seismic** conditions, the design displacement for the loading direction i-i is:

$$d_{Edi} = \pm 0.4 d_E + d_G \pm 0.5 d_T$$

where

- $d_E$  : design seismic displacement
- $d_G$  : displacement due to permanent or quasi-permanent actions
- $d_T$  : displacement due to temperature actions

$$d_{Ed} = \sqrt{d_{Edi}^2 + d_{Edj}^2}$$

where

- $d_{Edi}$  : Design displacement in main loading direction i-i
- $d_{Edj}$  : 30% of the design displacement in the lateral direction j-j

<b>Static combination</b>	<b>G±1.5×0.6 T ±1.5 BR</b>
Max negative	$d_{Edx} = -d_G - 1.50d_{BR} - 1.5 \cdot 0.6 d_{t(-37)} = -32.22$ mm
Max positive	$d_{Edx} = -d_G + 1.50d_{TR} + 1.5 \cdot 0.6 d_{t(+57)} = 34.46$ mm
<b>Seismic combination</b>	<b>G±0.4(Ex+0.30Ey)±0.5 T</b>
Max negative	$d_{Edx} = -0.4 d_E - d_G - 0.5 d_{t(-37)} = -55.05$ mm
Max positive	$d_{Edx} = 0.4 d_E - d_G + 0.5 d_{t(+57)} = 58.00$ mm

<b>Static combination</b>	<b>G±1.5×0.6 T ±1.5 BR</b>
Max negative	$d_{Edy} = -d_G - 1.50d_{BR} - 1.5 \cdot 0.6 d_{t(-37)} = 0.00$ mm
Max positive	$d_{Edy} = -d_G + 1.50d_{TR} + 1.5 \cdot 0.6 d_{t(+57)} = 0.00$ mm
<b>Seismic combination</b>	<b>G±0.4(0.30Ex+Ey)±0.5 T</b>
Max negative	$d_{Edy} = -0.4 d_E - d_G - 0.5 d_{t(-37)} = -78.46$ mm
Max positive	$d_{Edy} = 0.4 d_E - d_G + 0.5 d_{t(+57)} = 78.16$ mm
<b>Min displacements of the expansion joint</b>	
Static combination (x direction)	66.68 mm
Static combination (y direction)	0.00 mm

<b>Min gap</b>	
<b>COMBINATION</b>	<b>G±(Ex+0.30Ey)±0.5 T</b>
$d_{Ed} = d_E + d_G + 0.5d_{t(+57)} =$	114.69 mm
$d_{Ed} = -d_E + d_G - 0.5d_{t(+57)} =$	-111.63 mm

An expansion joint AGFLEXJ 140 ( $\pm 70$ ) or similar is chosen based on displacement calculation or an expansion joint AGFLEXJ 200 ( $\pm 100$ ) is chosen based on gap calculation.

### 3.7.3 Liquefaction case: Seismic scenario A ( $T_{ret}=1000y$ )

In this case a refined finite element model is also examined considering soil-structure interaction at the base of the piers. The finite element model of the bridge was described in Section 3.7.1. The only modification made is with regard to the dynamic impedance functions. The dynamic impedance functions at the footing-soil interface adopted for the liquefaction case were computed in Section 3.6.

#### 3.7.3.1 Horizontal liquefaction-induced differential displacements

According to the proposed methodology, except for the settlements and rotations due to liquefaction (Section 3.2), the superstructure should be able to accommodate the maximum liquefaction-induced differential horizontal displacements between the abutments and the adjacent piers. Due to the response spectrum method limitations, one and only spectrum can be applied to all the support points (i.e. pier footings and abutments) for each loading case. However, it is recognized that the seismic excitation differs significantly between the piers and the abutments since the latter are founded on non-liquefaction susceptible soil while the piers on potentially liquefiable soil. To overcome this inconsistency, additional displacements due to liquefaction are imposed to the footings of the piers.

Specifically, the expected level of the imposed horizontal displacements due to liquefaction  $\{\delta\}$  is defined as a separate loading case. The design value of the horizontal differential displacement is derived from the geotechnical study of the particular soil profile [Deliverable 4, WP04]. The peak and average transient displacements of the liquefied ground are summarized in **Table 3.8** [Deliverable 4, WP04]. The design value of the horizontal differential displacement is extracted from **Table 3.8** and is equal to 12.17cm.

**Table 3.8:** Peak and average transient displacements of the liquefied ground [Deliverable 4, WP04].

**Πίνακας 3.8:** Μέγιστες και μέσες εδαφικές μετακινήσεις ρευστοποιημένου εδάφους [Deliverable 4, WP04].

$\alpha/\alpha$	Excitation	Peak horizontal displacement, $\delta$ (cm)				
		Outcropping bedrock	Ground Surface			
			w/ improved top layer		w/o improved top layer	
			Absolute	Relative	Absolute	Relative
1	ITALY_BAG	13.13	19.12	10.49	27.64	20.59
2	ITALY_VLT	1.28	2.81	3.20	4.03	4.39
3	KOBE_TDO	13.47	17.17	20	14.46	21.47
4	LOMAP_AND	10.20	21.16	22.17	11.23	9.31
5	LOMAP_GIL	11.68	12.59	4.99	13.07	4.87
<b>average</b>		<b>9.95</b>	<b>14.57</b>	<b>12.17</b>	<b>14.09</b>	<b>12.13</b>

### ***Structural response under the liquefaction-induced imposed displacements and rotations***

The previously extracted displacements are then considered according to the combination rule:

$$\pm\delta_x \pm 0.30 \delta_y \quad [3.10]$$

$$\pm 0.30 \delta_x \pm \delta_y \quad [3.11]$$

where  $\delta_x$ ,  $\delta_y$  are the displacements along the longitudinal and the transversal bridge axis. These displacements are then further combined with gravity ( $G$ ), live ( $Q$ ) loads and seismic loads ( $E$ ) using the partial factors for actions according to the applied code (e.g. Eurocode 0). Finally, the following combinations of actions are examined:

(i) Case 1:

$$G + 0.2Q \pm E_x \pm 0.30E_y \pm 0.30E_z + 0.30 (\pm\delta_x \pm 0.30\delta_y)$$

$$G + 0.2Q \pm 0.30E_x \pm E_y \pm 0.30E_z + 0.30 (\pm 0.30\delta_x \pm \delta_y)$$

$$G + 0.2Q \pm 0.30E_x \pm 0.30E_y \pm E_z + 0.30 (\pm 0.30\delta_x \pm 0.30\delta_y)$$

(ii) Case 2:

$$G + 0.2Q + 0.30 (\pm E_x \pm 0.30E_y \pm 0.30E_z) + (\pm\delta_x \pm 0.30\delta_y)$$

$$G + 0.2Q + 0.30 (\pm 0.30E_x \pm E_y \pm 0.30E_z) + (\pm 0.30\delta_x \pm \delta_y)$$

$$G + 0.2Q + 0.30 (\pm 0.30E_x \pm 0.30E_y \pm E_z) + (\pm 0.30\delta_x \pm 0.30\delta_y)$$

The horizontal differential displacements were applied at the base of the piers in the (a) same and (b) opposite directions as shown in **Figures 3.15** and **3.16**, respectively.

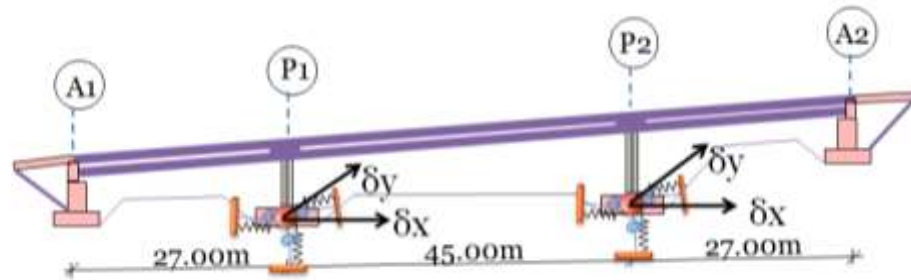


**Figure 3.15.** Liquefaction-induced differential displacements between piers and abutments (same application direction at the two piers).

**Σχήμα 3.15.** Διαφορικές μετακινήσεις μεταξύ βάθρων και ακροβάθρων λόγω ρευστοποίησης (κοινή διεύθυνση εφαρμογής στα δύο βάθρα).

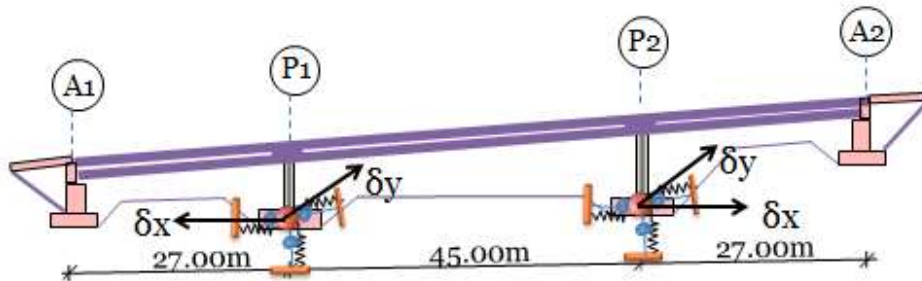


**Figure 3.16.** Liquefaction-induced differential displacements between piers and abutments (opposite application direction at the two piers).

**Σχήμα 3.16.** Διαφορικές μετακινήσεις μεταξύ βάθρων και ακροβάθρων λόγω ρευστοποίησης (αντίθετη διεύθυνση εφαρμογής στα δύο βάθρα).

*(a) Same application direction*

The deformed shape as well as the structural response (bending moments and axial forces) for the critical combinations of actions (a)  $G + 0.2Q + E_x + 0.30E_y + 0.30E_z + 0.30(\delta_x + 0.30\delta_y)$  and (b)  $G + 0.2Q + 0.30(E_x + 0.30E_y + 0.30E_z) + (\delta_x + 0.30\delta_y)$  are presented in **Figures 3.17** and **3.18**, respectively. It is seen that the maximum bending moments for the first combination of actions at the left and right piers are  $M=15,424\text{kNm}$  and  $M=11,250\text{kNm}$ , respectively. The maximum axial forces at the base of the two piers are  $N=-11,312\text{kN}$  and  $N=-10,847\text{kN}$ , respectively. For the second combination, the maximum bending moments at the left and right piers are  $M=10,778\text{kNm}$  and  $M=4,789\text{kNm}$ , respectively. The maximum axial forces at the base of the two piers are  $N=-10,917\text{kN}$  and  $N=-10,605\text{kN}$ , respectively. It is noted that axial forces in these combinations are lower than in those without  $\delta_x, \delta_y$ .

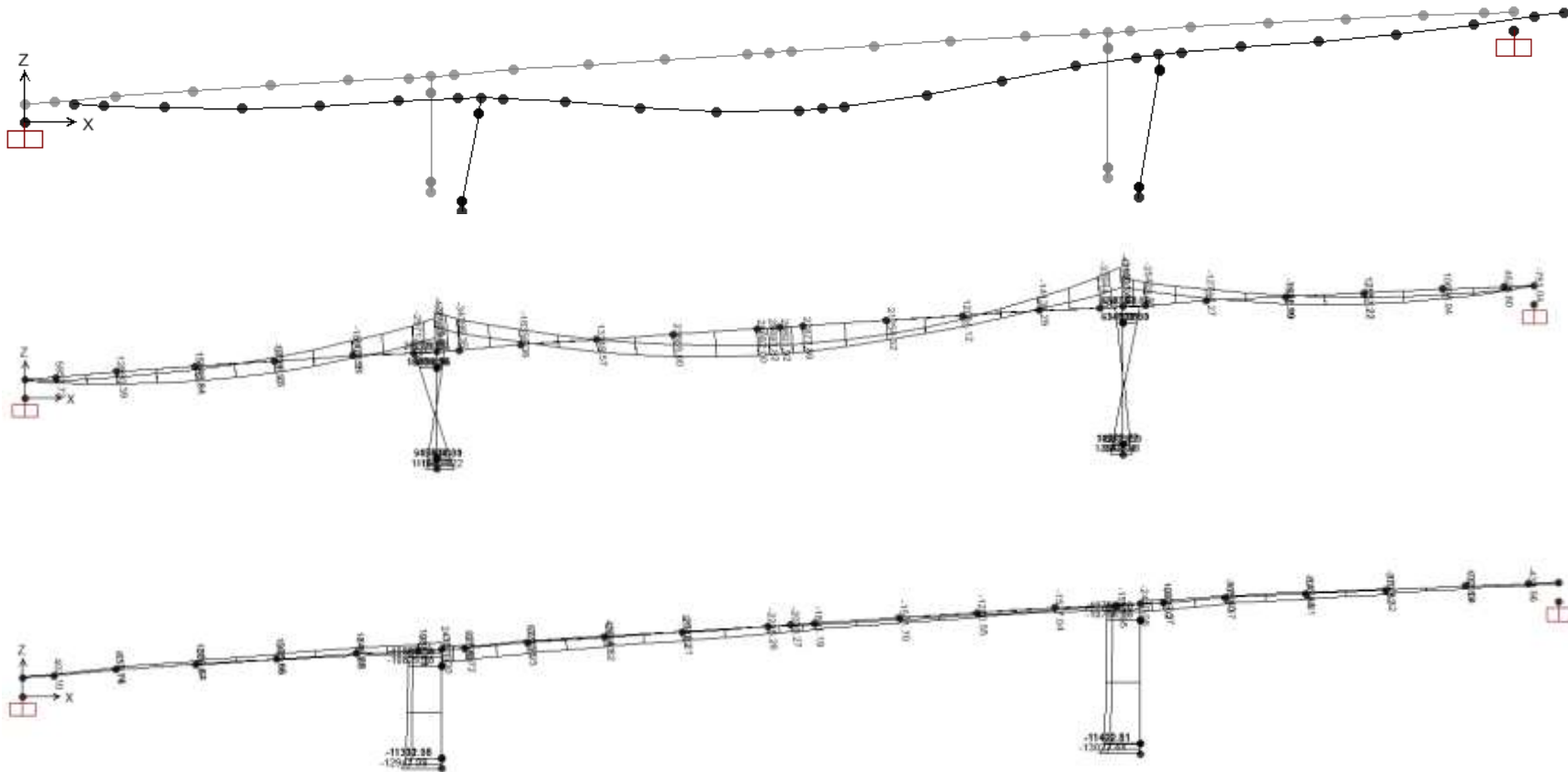


**Figure 3.17.** Deformed shape (top), bending moments (middle) and corresponding axial forces (bottom) acting at the bridge for the combination  $G + 0.2Q + Ex + 0.30Ey + 0.30Ez + 0.30(\delta x + 0.30\delta y)$  (units:  $kNm, N$ ).

**Σχήμα 3.17.** Παραμορφωμένη κατάσταση (πάνω), διάγραμμα ροπών (μέση) και αντίστοιχων αξονικών δυνάμεων (κάτω) που αναπτύσσονται στη γέφυρα για το συνδυασμό  $G + 0.2Q + Ex + 0.30Ey + 0.30Ez + 0.30(\delta x + 0.30\delta y)$  (μονάδες:  $kNm, N$ ).

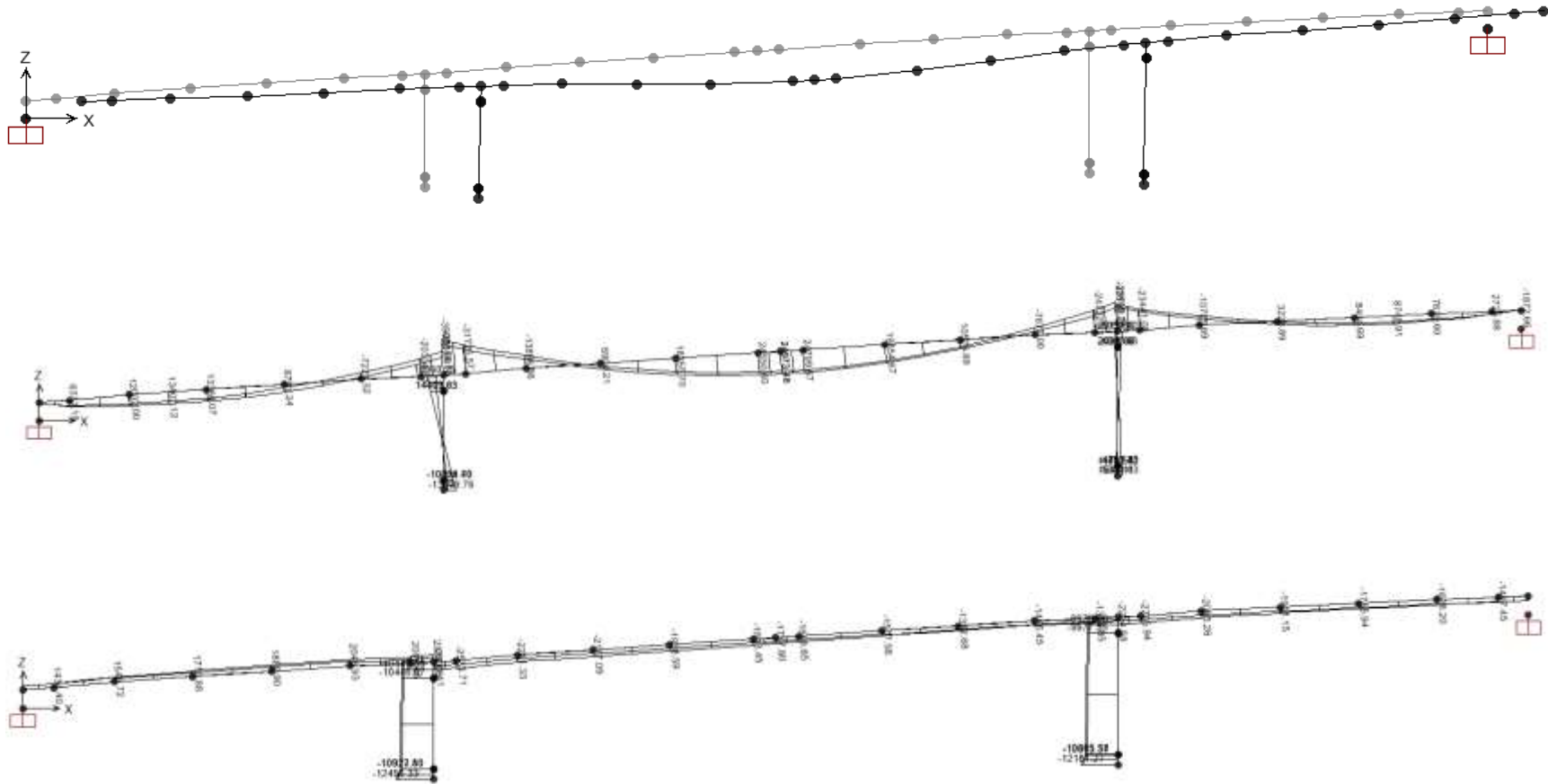


**Figure 3.18.** Deformed shape (top), bending moments (middle) and corresponding axial forces (bottom) acting at the bridge for the combination  $G + 0.2Q + 0.30 (Ex + 0.30Ey + 0.30Ez) + (\delta x + 0.30\delta y)$  (units:  $kNm, N$ ).

**Σχήμα 3.18.** Παραμορφωμένη κατάσταση (πάνω), διάγραμμα ροπών (μέση) και αντίστοιχων αξονικών δυνάμεων (κάτω) που αναπτύσσονται στη γέφυρα για το συνδυασμό  $G + 0.2Q + 0.30 (Ex + 0.30Ey + 0.30Ez) + (\delta x + 0.30\delta y)$  (μονάδες:  $kNm, N$ ).

It is also observed that the maximum response quantities ( $M$ ,  $V$ ,  $N$ ) for all the examined load combinations are more favourable compared to those of the non-liquefaction case. Hence, there is no need to redesign the bridge components. However, there is need to re-evaluate the tolerable settlements and rotations for the specific bridge (Section 3.2) since the required pier reinforcement derived by the conventional design (Section 3.1) differs significantly of that of the proposed methodology (Section 3.7).

Nonlinear static analysis was again performed for a predefined pattern ( $\Delta$ ) of displacements (settlements,  $\rho$ ) and rotations ( $\vartheta_x$ ,  $\vartheta_y$ ) which was applied at the base of the piers until the bridge 'collapses'. **Figure 3.19** presents the applied settlements at the base of piers as a function of the rotational ductility ( $\mu_\vartheta$ ) along with the adopted performance criteria associated with the acceptable damage level at the bridge. Specifically, for settlements ( $\rho$ ) smaller than 0.06m, no damage is expected in the bridge as it responds in the elastic range. For settlements in the range  $0.06 \leq \rho \leq 0.12\text{m}$ , minor damage is expected, while for settlements in the range  $0.12 \leq \rho \leq 0.20\text{m}$ , moderate damage is expected. Finally, the bridge "collapses" for imposed settlements greater than 0.20m. In this case, a value of 0.12m was adopted for the settlements at the base of piers corresponding to minor damage. By further assuming a safety factor of 1.15, the tolerable settlement was set equal to  $0.12/1.15=0.10\text{m}$ . It is noted that the corresponding tolerable dynamic settlement ( $\rho_{dyn}=\rho-\rho_{static}=0.10\text{m}-0.02\text{m}=0.08\text{m}$ ) is smaller than the dynamic settlement (0.057m) which was computed in Section 3.5.

Finally, the previously derived (Section 3.7.2)  $146\Phi 25$  ( $717\text{cm}^2$ ) are used for the longitudinal pier reinforcement, two sets of elastomeric bearings with dimensions 500x600mm are used at each deck end while an expansion joint AGFLEXJ 140 ( $\pm 70$ ) or similar is chosen based on displacement calculation or an expansion joint AGFLEXJ 200 ( $\pm 100$ ) on gap calculation.

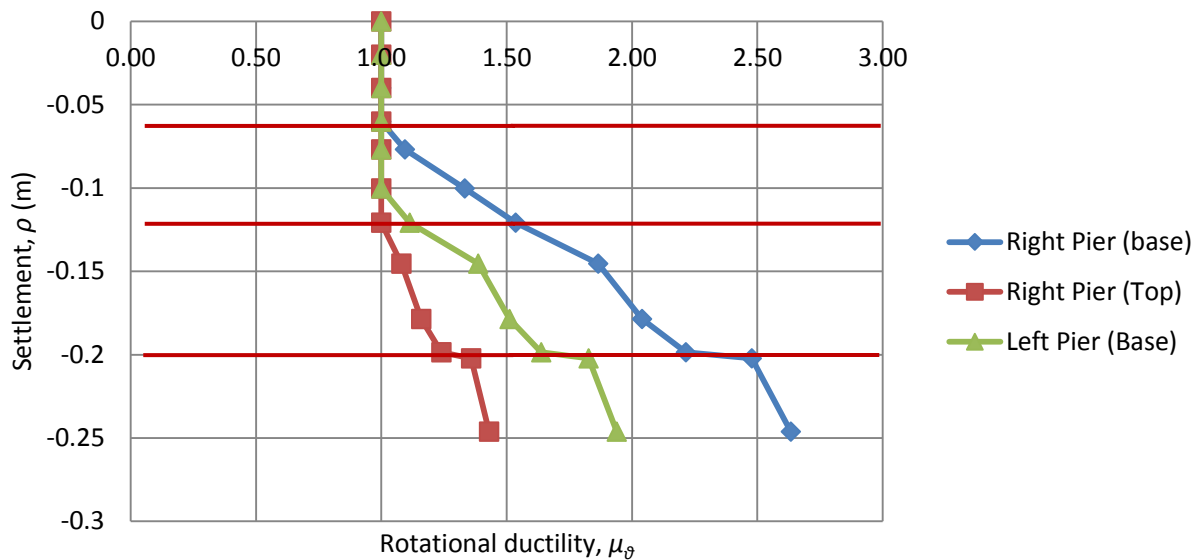


**Figure 3.19.** Applied settlements at the base of piers as a function of rotational ductility.

**Σχήμα 3.19.** Επιβαλλόμενες καθιζήσεις στη βάση των στύλων συναρτήσει της πλαστιμότητας στροφών.

*(b) Opposite application direction*

The deformed shape as well as the structural response (bending moments and axial forces) for the critical combinations of actions (a)  $G + 0.2Q + E_x + 0.30E_y + 0.30E_z + 0.30(\delta_x + 0.30\delta_y)$  and (b)  $G + 0.2Q + 0.30(E_x + 0.30E_y + 0.30E_z) + (\delta_x + 0.30\delta_y)$  are presented in **Figures 3.20** and **3.21**, respectively. It is shown that the maximum bending moments for the first combination of actions at the left and right piers are  $M=45,013\text{kNm}$  and  $M=50,766\text{kNm}$ , respectively. The maximum axial forces at the base of the two piers are  $N=-11,922\text{kN}$  and  $N=-13,354\text{kN}$ , respectively. For the second combination, the maximum bending moments at the left and right piers are  $M=115,562\text{kNm}$  and  $M=145,426\text{kNm}$ , respectively. The maximum axial forces at the base of the two piers are  $N=-12,949$  and  $N=-17,117\text{kN}$ , respectively.

It was found that the required amount of reinforcement is much greater than 4%, a value that is not acceptable according to the current codes provisions. Moreover, it is seen (**Figure 3.20, 3.21**) that the middle span responds mainly as a simply-supported beam which indicates that a different structural system (i.e. simply-supported prestressed beams) might be more

appropriate in this case (in the specific context of design against liquefaction).

It is therefore concluded that if the horizontal differential displacements are applied in opposite directions, the “natural” seismic isolation method is not appropriate for the statically indeterminate bridge studied.

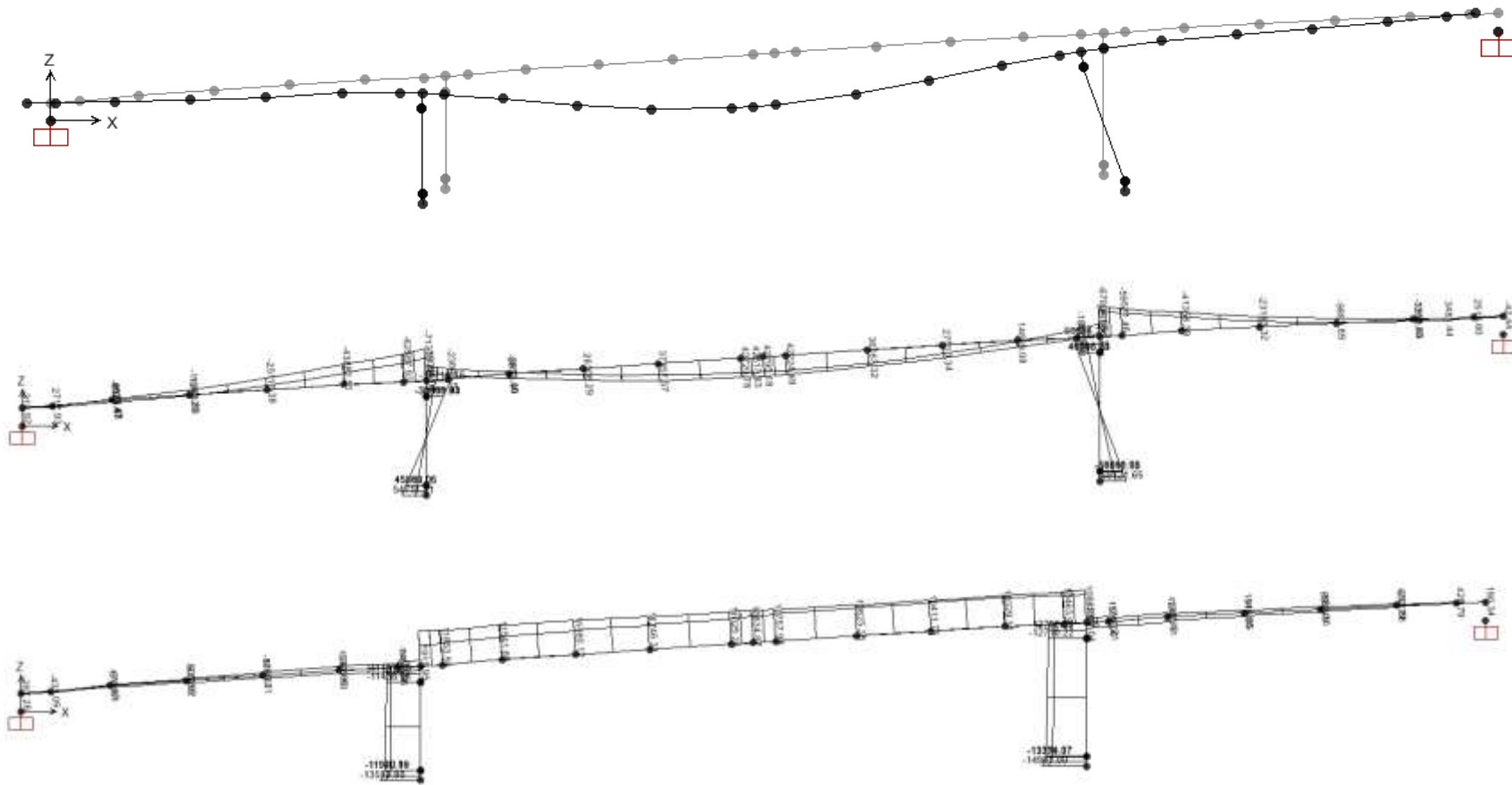


**Figure 3.20.** Deformed shape (top), bending moments (middle) and corresponding axial forces (bottom) acting at the bridge for the combination  $G + 0.2Q + Ex + 0.30Ey + 0.30Ez + 0.30(\delta x + 0.30\delta y)$  (units:  $kNm, N$ ).

**Σχήμα 3.20.** Παραμορφωμένη κατάσταση (πάνω), διάγραμμα ροπών (μέση) και αντίστοιχων αξονικών δυνάμεων (κάτω) που αναπτύσσονται στη γέφυρα για το συνδυασμό  $G + 0.2Q + Ex + 0.30Ey + 0.30Ez + 0.30(\delta x + 0.30\delta y)$  (μονάδες:  $kNm, N$ ).

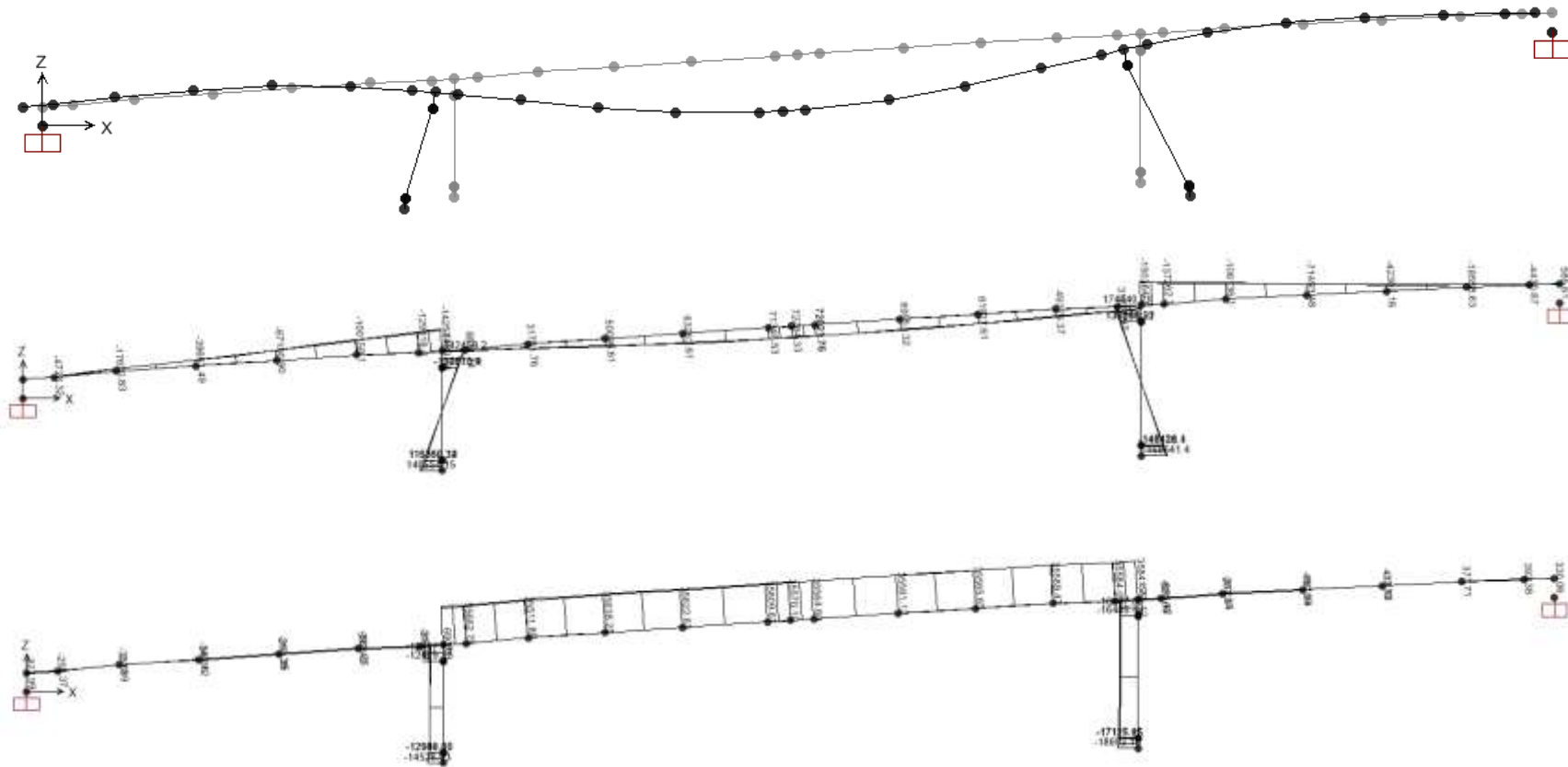


**Figure 3.21.** Deformed shape (top), bending moments (middle) and corresponding axial forces (bottom) acting at the bridge for the combination  $G + 0.2Q + 0.30 (Ex + 0.30Ey + 0.30Ez) + (\delta x + 0.30\delta y)$  (units:  $kNm, N$ ).

**Σχήμα 3.21.** Παραμορφωμένη κατάσταση (πάνω), διάγραμμα ροπών (μέση) και αντίστοιχων αξονικών δυνάμεων (κάτω) που αναπτύσσονται στη γέφυρα για το συνδυασμό  $G + 0.2Q + 0.30 (Ex + 0.30Ey + 0.30Ez) + (\delta x + 0.30\delta y)$  (μονάδες:  $kNm, N$ ).

## 4. Summary and Conclusions

---

The application of the proposed methodology for bridge design on liquefiable soils is presented in this deliverable for the case of a statically indeterminate RC bridge. The design process is tailored to the salient features of the novel soil isolation concept, while at the same time complying with the provisions of seismic codes. The procedure proposed herein, involves initial design of the foundation and the superstructure according to modern seismic codes (i.e. Eurocodes) after appropriate adaptations to account for the effect of liquefaction on the design seismic loads and displacements.

It was found that if the horizontal differential displacements are applied in opposite directions at the base of the piers, the “natural” seismic isolation method is not appropriate for use in the statically indeterminate RC bridge studied. On the contrary, if the differential displacements are applied in the same direction, footings of 9.0m×10.50m are required for the two piers along with an improved zone of 14.1m length, 5.5m depth corresponding to an improved soil volume equal to  $710.64m^3$ . Moreover, 146Ø25 (717cm<sup>2</sup>) are required for the longitudinal pier reinforcement while two sets of elastomeric bearings with dimensions 500x600mm are needed at each deck end. Finally, an expansion joint AGFLEXJ 200 (±100) is required based on gap calculation.

## 5. References

---

- Barker, R. M., Duncan, J. M., Rojiani, K. B., Ooi, P. S. K., Tan, C. K., and Kim, S. G. (1991). *Manuals for the Design of Bridge Foundations*, NCHRP Report 343, Transportation Research Board, National Research Council, Washington, DC.
- DiMillio, A. F. (1982). *Performance of Highway Bridge Abutments on Spread Footings on Compacted Fill*. Report No. FHWA RD-81-184, Federal Highway Administration, U.S. Department of Transportation.
- Gifford, D. G., Kraemer, S. R., Wheeler, J. R. και McKown, A. F. (1987). *Spread Footings for Highway Bridges*. Report No. FHWA RD-86-185, Federal Highway Administration, U.S. Department of Transportation.
- Mander J, Priestley M, Park R. *Theoretical stress-strain model for confined concrete*. Journal of Structural Engineering, 1988; 114 (8): 1804–1826. DOI: 10.1061/(ASCE)0733-9445(1988)114:8(1804).
- Mylonakis, G., Nikolaou, S., Gazetas, G. (2006). *Footings under seismic loading: Analysis and design issues with emphasis on bridge foundations*. Soil Dynamics and Earthquake Engineering, 26: 824-853.
- Naeim, F. and Kelly, J. (1999), *Design of Seismic Isolated Structures: From theory to practice*, John Wiley and Sons.
- Naresh, C., Samtani, N. C., Nowatzki, E. A. and Mertz, D. (2010). *Selection of Spread Footings on Soils to Support Highway Bridge Structures*. Report No. FHWA RD/TD-10-001, Federal Highway Administration, U.S. Department of Transportation.
- Poulos, H.G. and Davis, E. (1974). *Elastic solutions for soil and rock mechanics*. Wiley, New York.
- Samtani, N. C. and Nowatzki, E. A. (2006). *Soils and Foundations*. Vol. I and II, Report No. FHWA-NHI-06-088 and FHWA-NHI-06-089, Federal Highway Administration, U.S. Department of Transportation.
- Sargand and Masada (2006). *Further Use of Spread Footing Foundations for Highway Bridges*. State Job Number 14747(0) Final Report FHWA-OH-2006/8 Final Report to Ohio Dept. of Transportation.
- Sladen, J.A., D' Hollander, R.D., Krahn, J. (1985). *The liquefaction of sands, a collapse surface approach*. Canadian Geotechnical Journal, 22: 564-578.
- Wahls, H. E. (1983). *Shallow Foundations for Highway Structures*. NCHRP Report 107, Transportation Research Board, National Research Council, Washington, D.C.
- Wahls, H. E. (1990). *Synthesis of Highway Practice 159: Design and Construction of Bridge Approaches*, Transportation Research Board, National Research Council, Washington, D.C.

### Codes and Standards

- AASHTO (2002). Standard Specifications for Highway Bridges. American Association of State Highway and Transportation Officials, Washington, D.C.
- AASHTO (2007 with 2009 Interims). AASHTO LRFD Bridge Design Specifications. 4th Edition, American Association of State Highway and Transportation Officials, Washington, D.C.
- EN 1990: 2002 Eurocode 0: Basis of Structural Design, European Committee for Standardization, Brussels.
- EN 1992-2:2005. Design of concrete structures - Part 2: Concrete bridges. European Committee for Standardization, Brussels.
- EN1337-1: Structural bearings – Elastomeric bearings. European Committee for Standardization, Brussels.
- EN 1997-1:2004. Geotechnical design - Part 1: General rules. European Committee for Standardization, Brussels.
- EN 1998-1:2004. Design of structures for earthquake resistance - Part 1: General rules, seismic actions and rules for buildings. European Committee for Standardization, Brussels.
- EN 1998-2:2005. Design of structures for earthquake resistance - Part 2: Bridges. European Committee for Standardization, Brussels.
- EN 1998-3:2005. Design of structures for earthquake resistance - Part 3: Assessment and retrofitting of buildings. European Committee for Standardization, Brussels.
- EN 1998-5:2005. Design of structures for earthquake resistance - Part 5: Foundations, retaining structures and geotechnical aspects. European Committee for Standardization, Brussels.
- FEMA-356 (2000). Prestandard and Commentary for the Seismic Rehabilitation of Buildings. ASCE, FEMA, Washington, D.C.
- FHWA (1987) Spread Footings for Highway Bridge, Report No. FHWA RD-86-185, Authors: Gifford DG, Kraemer SR, Wheeler JR and McKown AF, Federal Highway Administration, U.S. Dept of Transportation.
- FHWA (1982) Performance of Highway Bridge Abutments on Spread Footings on Compacted Fill, Report No. FHWA RD-81-184, DiMillio AF, Federal Highway Administration, U.S. Department of Transportation.

### Research program THALIS-NTUA Deliverables

- Bouckovalas, G., Karamitros, D., Chaloulos, Y., Vavourakis, V. and Chatzicharalambous, E. (2014). *Technical Report*. Research program THALIS-NTUA: Innovative design of bridge piers on liquefiable soils with the use of natural seismic isolation - Analytical methodology for the design of shallow foundations on liquefiable soil. [Deliverable 3, WP03].
- Bouckovalas, G., Loukidis, D., Chaloulos, Y., Tsiapas, Y. and Chatzicharalambous, E. (2014). *Technical Report*. Research program THALIS-NTUA: Innovative design of

## REFERENCES

---

bridge piers on liquefiable soils with the use of natural seismic isolation - Design for liquefiable ground. [Deliverable 4, WP04]

Mylonakis, G., Bouckovalas, G., Karatzia, X., Tsiapas, Y. and Chatzicharalambous, E. (2014). *Technical Report*. Research program THALIS-NTUA: Innovative design of bridge piers on liquefiable soils with the use of natural seismic isolation - Soil springs and dashpots for footings on liquefiable soil. [Deliverable 5, WP05]

Kappos, A., Sextos, A, Taskari, O. and Mylona, E.-K. (2014). *Conventional design of a statically indeterminate RC bridge*. Research program THALIS-NTUA: Innovative design of bridge piers on liquefiable soils with the use of natural seismic isolation – Application to statically indeterminate RC bridges. [Deliverable 7a, WP07]

Kappos, A., Sextos, A, Taskari, O. and Mylona, E.-K. (2015). *Performance criteria for statically indeterminate bridges*. Research program THALIS-NTUA: Innovative design of bridge piers on liquefiable soils with the use of natural seismic isolation – Application to statically indeterminate RC bridges [Deliverable 7b, WP07]